Scholars' Mine

Doctoral Dissertations   Student Theses and Dissertations

2014

A generalized optimal power flow program for distribution system analysis and operation with distributed energy resources and solid state transformers

Fanjun Meng

Follow this and additional works at: https://scholarsmine.mst.edu/doctoral_dissertations

Part of the Electrical and Computer Engineering Commons

Department: Electrical and Computer Engineering

Recommended Citation

A GENERALIZED OPTIMAL POWER FLOW PROGRAM

FOR DISTRIBUTION SYSTEM ANALYSIS AND OPERATION

WITH DISTRIBUTED ENERGY RESOURCES AND

SOLID STATE TRANSFORMERS

by

FANJUN MENG

A DISSERTATION

Presented to the Faculty of the Graduate School of the

MISSOURI UNIVERSITY OF SCIENCE AND TECHNOLOGY

In Partial Fulfillment of the Requirements for the Degree

DOCTOR OF PHILOSOPHY

in

ELECTRICAL ENGINEERING

2014

Approved
Dr. Badrul Chowdhury, Advisor
Dr. Mariesa Crow
Dr. Jonathan Kimball
Dr. Mehdi Ferdowsi
Dr. Bruce McMillin

PUBLICATION DISSERTATION OPTION

This dissertation has been prepared in the form of three papers for publication. The first paper consisting of pages 4 to 33 has been published in *IEEE Transactions on Smart Grid,* vol. 4, no. 4, Dec 2013. The second paper consisting of pages 34 to 64 will be submitted for publication in *IEEE Transaction on Smart Grid*. The third paper consisting pages 65 to 102 will be submitted for publication in *IEEE Transaction on Power Delivery*.

ABSTRACT

The present distribution system is gradually trending towards a smart grid paradigm with massive development of distributed energy resources (DER), advanced power electronics interfaces, and a digitalized communication platform. Such profound changes bring challenges as well as opportunities for an entity like the distribution network operator (DNO) to optimally operate DERs and other controllable elements to achieve higher levels of energy efficiency, economic benefits, supply reliability and power quality.

The major contribution of this dissertation is in the development of a generalized three-phase optimal power flow (OPF) program in a novel control scheme for future distribution system optimization and economic operation. It is developed based on primal-dual interior point method (PDIPM). The program is general enough to model comprehensive system components and topologies. The program can also be customized by user-defined cost functions, system constraints, and new device, such as solid state transformers (SST). An energy storage optimal control using dynamic programming is also proposed to coordinate with the OPF based on a pricing signal called the distribution locational marginal price (DLMP). The proposed OPF program can be used by the DNO in an open access competitive control scheme to optimally aggregate the energy mix by combining the profitability of each resource while satisfying system security constraints.

ACKNOWLEDGMENTS

I would like to express my appreciation to my advisor, Dr. Badrul Chowdhury, for offering me the freedom and enlightening advice as I started from an idea to a completed work. His thoughts and style of working have inspired me to pursue academic research based on a solid foundation of practical application. I would also like to thank my advising committee of Dr. Mariesa Crow, Dr. Jonathan Kimball, Dr. Mehdi Ferdowsi and Dr. Bruce McMillin for their instrumental support and valuable suggestions that I have incorporated into my research.

I would like to thank my lab mates and friends for being supportive and sharing all the joyful memories with me through the many years of life in Rolla. I would also like to thank my colleagues from partner campuses for their effort and collaboration during my work on the FREEDM project.

Most of all, I want to give my deepest gratefulness to my father, Mr. Zhihe Meng, my mother, Mrs. Lidong Sun and my wife, Mrs. Lijia Liao. I could never accomplish this long journey without your warmest love and faith in me.

TABLE OF CONTENTS

LIST OF ILLUSTRATIONS

Page

LIST OF TABLES

Page

1. INTRODUCTION

The electric power industry in the U.S., Europe and many other parts of the world have gradually transformed from regulated operation into a competitive environment at the transmission and sub-transmission levels since the evolutionary restructuring efforts of the early 1990's. However, the distribution system, which provides direct energy supply to customers through medium and/or low voltage feeders, has remained essentially unchanged with aging equipment and monopoly operation scheme. The concept of smart grid (SG) envisions future power systems, including distribution level, with higher energy efficiency, financial profitability, and reliability that will contribute to society's economic benefits and environmental health.

The distribution systems of today are beginning to feel the urgency to adopt a vastly different operational paradigm wherein an entity like a distribution network operator (DNO) can take a more active role in command under the advocacy of increasing DER and DES installations and better financial benefits as well as quality of energy service to customers. In addition, increased utilization of advanced power electronics, e.g. solid state transformer (SST), provide controllable var support and plug-and-play accessibility for distributed elements; and digitalized data communication using smart meters and phasor measurement units (PMU) are starting to become more common features of the smart distribution network.

The developments in hardware infrastructure enables, and also necessitates, a novel control scheme and regulatory policy for the DNO to optimally manage the myriad types of resources. Therefore, a three-phase optimal power flow (OPF) algorithm, as the main contribution of this dissertation, is developed to solve for constrained optimal

dispatch and operation of DERs and SSTs to minimize the total generation costs from aggregated transmission supply and DERs. This optimal control scheme is carried out in three parts:

The first part, presented in the first paper, introduces an optimal control scheme in single-phase equivalent distribution systems using a distribution locational marginal pricing (DLMP) index. The DLMP is obtained through OPF algorithm and used as a control signal to optimize the day-ahead operation planning of DER and DES.

In the second paper, an unbalanced three-phase OPF algorithm, which is mostly lacking in the present distribution system control, is proposed and tested for providing economic dispatch of transmission and DER suppliers. The algorithm is developed based on the PDIPM considering comprehensive system models and security constraints on nodal voltage magnitudes and line loading. It is also capable of solving for line loading management and generation re-dispatch in a looped or meshed system topology. Two alternative ways – nodal power balance method (PBM) and current injection method (CIM) – are adopted and compared in OPF formulation and performance.

The third paper focuses on the customization of the OPF algorithm to cooperate user-defined cost functions and new devices (e.g. SST) by automatically modifying variables, constraints and objective functions as needed. Particularly, the SSTs are integrated as controllable var support sources that will be optimally controlled by DNO using OPF program. The impacts from SST to OPF formulation and system operation is studied.

Simulation results present fast convergence to optimal solution of standard test systems with various configurations and topologies. Besides the main features of

economic control of DERs and congestion management, the proposed OPF program also shows potential for short or long term system optimal design.

PAPER

I.   Distributed Generation and Storage Optimal Control

with State Estimation

F. Meng, Student Member, *IEEE*, D. Haughton, Student Member, *IEEE*,

B. Chowdhury, Senior Member, *IEEE*, M. L. Crow, Fellow, *IEEE*, and G. T. Heydt, Life Fellow, *IEEE*

Abstract – **The increasing demand coupled with expanding installation of distributed resources call for the development of smart technologies to control and optimize distribution system operations. In this paper, a distributed generation and storage optimization algorithm is proposed using pricing signals as distribution locational marginal pricing (DLMP). This signal is used to optimize the day-ahead operation planning of distributed generation and energy storage. A distribution level state estimation algorithm is also designed. The main conclusion is that the proposed optimal control and state estimation will improve the energy efficiency and economic benefits in a digitally controlled distribution power system.**

Index Terms—**Digital system control, distributed resource optimization, distribution locational marginal prices, solid state controllers, state estimation.**

I. INTRODUCTION AND MOTIVATION

The electric power system was constructed more than a century ago with a vertical structure wherein electric power is generated at several large scale central power plants and transferred via long distance high voltage transmission lines to customers residing mostly in lower voltage distribution systems. The smart grid envisions future

power systems with higher reliability, availability, and efficiency that will contribute to society's economic and environmental health. While mostly lacking in the present power systems, smart grid technologies are undergoing fast development and integration in recent years due to government incentives and private investments. This design philosophy is intended to upgrade or replace robust overbuilding and the conservation of economic resources. The main benefits associated with this evolution include more efficient electricity transmission and delivery, reduced energy costs for utilities and consumers, reduced peak demands, increased penetration of renewable energy systems, and better integration of customer owned distributed generation systems [1].

Renewable generation technologies (e.g., photovoltaic and wind turbines) have become mature in recent years. The present research is pushing the envelope of solar energy harvesting and product development to fill the market from residential applications to central-station solar farms [2]. Energy storage in distribution class applications is a relatively new technology, but is undergoing rapid commercialization in a variety of forms including community battery storage facilities. In this context, evolutionary changes in the regulatory and traditional utilities have opened new opportunities for on-site power generation and energy management by consumers in distribution systems as a promising option to satisfy the demand growth as well as to improve reliability, power quality, and economically operate the power system.

These technology trends necessitate more advanced control methods to operate the increasing number of distributed re-sources. In this paper, an optimal control scheme for distributed renewable generation and energy storage is proposed using a distribution locational marginal pricing index (DLMP). The concept of DLMP is introduced to define

the marginal cost to supply an additional unit of demand in a distribution system [3]. The DLMPs are derived based on the day-ahead hourly optimal dispatch of generations, and are used for energy storage management; a distribution level state estimation provides near real-time system status which can be used to re-dispatch re-sources. This control scheme pro vides potential improvement for renewable energy harvest and economic benefits to both the customers and the utility.

II. ENVISIONED FUTURE DISTRIBUTION SYSTEMS

Contemporary distribution systems serve a variety of end user types and contain a variety of transformer connections, have limited control options such as voltage regulators, switched shunt capacitor banks, and tap changing transformers. The bi-directional communications capability between customers and the utility control center is also missing in the scheme. Therefore, system modeling and implementation of power and energy management using near real-time customer behavior has been limited. The future distribution system is envisioned to have the following main features that enhance options for system optimization and control.

A. High Penetration of Distributed Energy Resources

Presently, various forms of distributed energy resources have become a promising option for utility and consumers to serve the increasing demand at a cheaper cost and higher quality. For example, PV system installation in the U.S. had a rapid increase after the year 2000 and reached more than 2.5 GW by 2010, of which 2.1 GW were grid-connected. The annual PV installation grew 102% from 435 MW in 2009 to 878 MW in 2010 [4].

B. Advanced Solid State Controller

Many distributed generation and storage resources such as photovoltaic, wind, battery storage and plug-in-electric vehicles, cannot be directly connected to utility services. Solid state controllers are required as interconnection that can improve distributed resources integration by performing AC and DC power conversion and voltage regulation. One such technology—the solid state transformer (SST)—is proposed by the FREEDM Engineering Research Center, a National Science Foundation Engineering Research Center [5]. The main features include plug-and-play functionality f or generation and storage at the customer end, power factor regulation, and voltage support. The SST may eventually replace or supplement conventional distribution transformers.

C. Incentives and Market Opportunities for Distributed Resources

Many pricing programs are currently offered by utilities to encourage consumers to utilize renewable generation and manage energy usage. The net metering and feed-in-tariff programs allow consumers to accumulate credits for excess power generation over consumption. Another example is time-of-use (TOU) program that provides multiple electricity rates during different periods of day. This would encourage customers to shift energy usage from on-peak to off-peak period using distributed generation and energy storage.

Note that the competitive retail power market is one of the new phenomena in power sector restructuring. Individual consumers can select power suppliers in a given market. The emergence of green power suppliers are allowed to sell renewable energy usually at a premium as independent power producer [6]. Since the aforementioned

pricing policies are usually regulated by monopolistic utilities, the competitive open market in retail level will provide end users a better chance to earn higher benefits from self-generation. This would surely encourage distributed generation development and may lower the supply required from conventional thermal generations. To maintain a healthy market, both independent customers and utilities should benefit from higher penetration of distributed generation in the aspects of reduced energy costs, reduced transmission losses, reduced land use for central power plants and transmission lines, increased system reliability, and an overall improved environment [7].

D. Distribution Management Systems (DMS)

The control of future distribution systems will be based on a digitalized and computerized platform. The DMS, integrated at the substation level, utilizes the sensory and communications infrastructure envisioned as part of a Smart Grid to achieve optimized operations. Examples of DMS functions include switching automation, voltage profile optimization, selective networking to manage power flows, demand response, and system control. State estimation is envisioned as a critical component of future DMS to allow control based on near real-time operation condition instead of historical or forecasted data.

Utilizing real-time data has the potential to significantly enhance distribution planning and operations. A distribution class state estimation algorithm designed for three-phase networks with distributed generation, distributed storage, significant unbalance, and possible integration of solid state controllers is developed in [14]. The mathematical foundation for this algorithm is reviewed here, and illustrative examples of applications are presented in this paper.

III. DISTRIBUTED GENERATION AND STORAGE MANAGEMENT

As distributed power and energy penetration increases, new opportunities, as well as challenges, have been raised to optimize operation of such elements. Two levels of control paradigms are proposed for different types of customers.

A. *Distributed Generation as Independent Power Producer*

The distributed generation units used to have very low penetration and were generally never dispatched in generation planning. In this paper, we extend the optimal power flow (OPF) methodology, which is typically used in transmission networks, to substation control center so as to dispatch energy supply from legacy grid at transmission side as well as distributed self-generations, with the most competitive offer prices to serve the demand. It is most applicable to the commercial and industrial users who can invest in relatively larger distributed generation units (100 kW to the MW level) and are willing to participate in the competitive retail energy market.

Assume a steady-state power system at a specific time period, and that the power demands are known from forecast and remain constant during this period. The objective function F in (1) is to minimize the total power production costs from all dispatched generations. The active power generation cost function C_i is assumed to be quadratic or piecewise. The quantity $P_{G,i}$ is the active power injection from generation unit at node i.

$$\text{Min } F = \sum_{i=1}^{all\ generations} C_i(\mathrm{P}_{G,i}) \tag{1}$$

And the constraints are,

$$G_i = -P_{G,i} + P_{D,i} + \sum_{i \neq j} V_i V_j (\mathrm{G}_{ij} \cos \theta_{ij} + \mathrm{B}_{ij} \sin \theta_{ij}) \tag{2}$$

$$Q_i = -Q_{G,i} + Q_{D,i} + \sum_{i \neq j} V_i V_j (\mathrm{G}_{ij} \sin \theta_{ij} - \mathrm{B}_{ij} \cos \theta_{ij}) \tag{3}$$

$$H_k = LF_k - LF_k^{MAX} \leq 0 \tag{4}$$

$$P_{G,i}^{MIN} \leq P_{G,i} \leq P_{G,i}^{MAX} \tag{5}$$

$$V_i^{MIN} \leq V_i \leq V_i^{MAX} \tag{6}$$

G_i and Q_i are the active and reactive power balance constraints at each node $i=1,2,\ldots,N$, where $P_{D,i}$ and $Q_{D,i}$ are active and reactive power demand at node i, and the last terms in both (2) and (3) represent the active and reactive power flows from all connecting branches including the losses. H_k is the branch flow limit constraints at each branch $k=1,2,\ldots,M$, and LF_k is the line flow. (5) and (6) are active power generation capacity constraints and bus voltage magnitude limits respectively.

We introduce λ_i and μ_k as Lagrange multipliers and dual variables for power balance and line flow limit respectively and create the Lagrangian L:

$$L = F + \sum_{i=1}^{N} \lambda_i G_i (P_{G,i}) + \sum_{k=1}^{M} \mu_k H_k \tag{7}$$

A mathematical theory of solving the non-linear optimization problem using interior point method is described in [8], and such applications to solve optimal power flow (OPF) problem are described in [9], [10]. In this method the optimum point (x^*, P_G^*) is found while satisfying the constraints (2–6), where x^* is the vector of system dependent variable (e.g., voltage magnitude and angle) and P_G^* is a vector of controllable variance of active power injections from generation units. The Karush-Kuhn-Tucker (KKT) optimum point [8] is described as:

$$\left.\frac{\partial L}{\partial P_G}\right|^* = \left.\frac{\partial F}{\partial P_G}\right|^* - \lambda^* = 0 \tag{8}$$

$$\left.\frac{\partial L}{\partial \lambda}\right|^* = -P_G^* + P_D + G(x^*, P_G^*) = 0 \tag{9}$$

$$\mu^* \cdot H\left(x^*, P_G^*\right) = 0 \tag{10}$$

where λ^* is the vector of corresponding multipliers for nodal power balance which is determined in (8). Note that μ^* (≥ 0) are multipliers bound to line flow limit constraints and μ^* would be zero if the line flow constraint is satisfied.

The concept of distribution locational marginal price (DLMP) is introduced as an analog to the transmission LMP to describe the incremental cost to supply an additional unit of demand at a node in a distribution system. The DLMP can be derived as a dual variable from the OPF result and can be decomposed into three parts as marginal energy cost (MEC), marginal loss cost (MLC), and marginal congestion cost (MCC). The DLMP δ_i at each node i is decomposed as:

$$\delta_i = \delta_i^E + \delta_i^L + \delta_i^C = \lambda_i^* + \lambda_i^* \cdot \sum_{k=1}^{M} \frac{\partial P_{LOSS,k}}{\partial P_{G,i}} + \sum_{k=1}^{M} \mu_k^* \cdot \frac{\partial LF_k}{\partial P_{G,i}} \tag{11}$$

• MEC of DLMP

In many transmission LMP formulation approaches, a reference energy cost is selected out of the vector of λ^* according to the selection of reference node or other principles [10]. But here, all elements in the vector λ^* are used to represent the energy cost at each node in the distribution system, that is, $\delta_i^E = \lambda_i^*$.

• MLC of DLMP

The loss cost is the production of energy cost δ_i^E with the summation of loss factors at node i. The loss factor (also known as penalty factor) $LF_{k,i} = \partial P_{LOSS,k} / \partial P_{G,i}$ describes the incremental active power loss in line due to a net power injection (or consumption) at node i. An approximation of the loss factor is given as,

$$\begin{aligned} LF_{k,i} &= \frac{\partial P_{LOSS,k}}{\partial P_{G,i}} = \frac{\partial I_k^2 R_k}{\partial P_{G,i}} = 2I_k R_k \frac{\partial I_k}{\partial P_{G,i}} \\ &\approx \frac{2I_k R_k}{V_i \rho_i} \cdot \frac{\partial I_k}{\partial I_i} \approx \frac{2I_k R_k}{V_i \rho_i} \cdot \frac{\partial LF_k}{\partial P_{G,i}} = \frac{2I_k R_k}{V_i \rho_i} \cdot PTDF_{k,i} \end{aligned} \tag{12}$$

where V_i is the voltage magnitude at node i; ρ_i is the power factor of net injection; and $PTDF_{k,i} = \partial LF_k / \partial P_{G,i}$ is the power transfer distribution factor, similar to generation shift factor (GSF), which describes the change in line flow LF_k due to an incremental active power injection $\partial P_{G,i}$ at node i [12]. A linear approximation of $PTDF_{k,i}$ is given in (13). The x_k is the reactance of line k, from node s to t; and X_{si} are X_{ti} imaginary parts of the corresponding elements in the impedance matrix.

$$PTDF_{k,i} = \frac{\partial LF_k}{\partial P_{G,i}} = \frac{\partial}{\partial P_{G,i}}\left(\frac{\theta_s - \theta_t}{x_k}\right) = \frac{X_{si} - X_{ti}}{x_k} \tag{13}$$

An alternative way to calculate the loss factor is derived based on the fast decoupled AC power flow method. It is assumed that an incremental power injection at node i will be compensated at the slack node n. So the resulting line loss in line k can be formulized as:

$$\Delta P_{LOSS,k} = \begin{bmatrix} \dfrac{\partial P_{LOSS,k}}{\partial \overline{V}} & \dfrac{\partial P_{LOSS,k}}{\partial \overline{\theta}} \end{bmatrix} \cdot \begin{bmatrix} \overline{V} \\ \overline{\theta} \end{bmatrix} = \begin{bmatrix} \dfrac{\partial P_{LOSS,k}}{\partial \overline{V}} & \dfrac{\partial P_{LOSS,k}}{\partial \overline{\theta}} \end{bmatrix} \cdot \begin{bmatrix} J_{11}^{-1} & J_{12}^{-1} \\ J_{21}^{-1} & J_{22}^{-1} \end{bmatrix} \cdot \begin{bmatrix} \Delta \overline{P} \\ \Delta \overline{Q} \end{bmatrix} \tag{14}$$

where $\overline{V}$ and $\overline{\theta}$ are vectors of bus voltages and angles; $\overline{P}$ and $\overline{Q}$ are vectors of net bus power injections; J_{ij}^{-1} $(i, j = 1, 2)$ are block sections of the inverse of the Jacobian matrix J^{-1} based on the decoupled technique.

Reformulate (14) to get the loss factor $LF_{k,i}$ as:

$$LF_{k,i} = \frac{\partial P_{LOSS,k}}{\partial P_{G,i}} = \frac{\partial P_{LOSS,k}}{\partial \overline{V}} \cdot J_{11}^{-1} + \frac{\partial P_{LOSS,k}}{\partial \overline{\theta}} \cdot J_{21}^{-1} \tag{15}$$

Irrespective of whether (12) or (14) is used, the calculation of MLC will be affected by the selection of slack bus since it is assumed that the additional power injection at the present node will be compensated by the slack bus. This might not hold in the case of a

microgrid or islanded operations. It is assumed that the transmission feed is still available and the substation node is considered as the slack bus.

• MCC of DLMP

The congestion cost is the summation of the products of μ_k^* and $PTDF_{k,i}$. Instead of (13), the $PTDF_{k,i}$ can also be found using a similar technique as in (15). The μ_k^* would be zero if line k is not congested. It is true that congestion is not likely in the present distribution systems since the systems are usually built with enough capacity margins on feeders and laterals, and the system is secured even during coincident peak demands. The congestion term is still kept for the following reasons: 1) the MCC could be used as reference signal for switching automation in DMS as mentioned in Section II-D. 2) the increasing penetration from distributed resources may affect the coincident maximum line flows in either directions and create unexpected congestions; so the MCC can identify and quantify such phenomenon and target the nodes for re-dispatch or line switching.

• Utilization of DLMP

The DLMPs reveal the marginal supply costs at each node. These pricing signals could be used as a control reference in multiple functions: 1) serve as reference pricing index for participants in a competitive retail market operation; 2) to be used as dynamic pricing profiles for energy storage management, as dis-cussed in Section III-B; 3) to provide valuable information for infrastructure expansion or resources allocation based on statistical analysis of pricing indices.

B. *Distributed Energy Storage Management*

The energy storage management is one of the key technologies for electricity users to actively participate in system operations and earn a variety of benefits. Customers who own small scale distributed generation (kW level) and energy storage (e.g., community battery storage) can monitor the local demand, renewable generation and system energy pricing signal (e.g., DLMP), thereby mange the energy storage to shift their electricity usage in a 24-hour period in order to reduce the electricity bills or achieve other benefits.

The day-ahead energy management procedure has two objective functions. The primary objective function F_1 is to minimize the total daily energy bill for individual customers (16). We divide the 24-hour period into multiple stages $K=1,…,M$. A steady state system operation is assumed and all variables remain unchanged within each stage. The $price(K)$ is the dynamic energy price at stage K; $P_{grid}(K)$ is the net power withdrawn from grid; and ΔT is the time duration of each period, e.g., one hour.

$$\text{Min} \qquad F_1 = \sum_{k=1}^{M} price(K) \cdot P_{grid}(K) \cdot \Delta T \qquad\qquad (16)$$

The secondary objective function F_2 is needed to minimize the variance of grid power (net power demand) through a 24-hour period. The term $\overline{P_{grid}}$ is the average of net grid power based on forecasted profile. Although F_2 does not show a direct benefit to energy bill saving, optimizing towards this objective will help reduce the peak of daily net demand and raise the valley. This may help reduce the risk of switching on and off the thermal units at the transmission side, which reduces the chances of dispatching expensive and less efficient generation units. Hypothetically, it also improves renewable energy harvest and efficiency, e.g., for photovoltaic systems. Photovoltaic systems

naturally have peak production at off-peak hours when energy cost is lower, but zero production during evening on-peak hours. The formulation of F_2 is,

$$\text{Min} \quad F_2 = \sum_{k=1}^{M} \left(\left\| P_{grid}(K) - P_{grid} \right\| \right) \tag{17}$$

Constraints:

$$P_{grid} = \begin{cases} P_{LOAD} - P_{DG} - P_b \cdot \eta_{disch} & \text{when discharging} \\ P_{LOAD} - P_{DG} - P_b \cdot \dfrac{1}{\eta_{disch}} & \text{when charging} \end{cases} \tag{18}$$

$$SOC^{MIN} \leq \text{SOC}(K) \leq SOC^{MAX} \tag{19}$$

$$P_b^{MIN} \leq P_b(K) \leq P_b^{MAX} \tag{20}$$

$$cyc_{ch} \leq cyc_{ch}^{MAX} \quad \text{and} \quad cyc_{disch} \leq cyc_{disch}^{MAX} \tag{21}$$

$$SOC(k+1) = SOC(k) + P_b(k) \cdot \Delta T / E_b \cdot 100\% \tag{22}$$

Equation (18) gives the power balance constraint, where P_b is control variable of the battery charge/discharge power seen at battery terminal; grid power P_{grid} is a dependent variable; the load P_{LOAD} and distributed generation P_{DG} are forecasted values; η_{ch} and η_{disch} (<1) are the overall charge/discharge efficiency of charging converters and battery system. Equations (19) and (20) are constraints for the battery stage of charge (SOC) and battery power. The SOC limits are set to prevent overcharging or depletion, the lower bound limit also guarantees emergent service to critical load during contingency. A limit on charge/discharge cycle (21) is necessary to extend battery life cycle [11]. The SOC is updated in (22) for every next stage. E_b is the battery energy capacity in kWh.

The optimization algorithm is developed based on the classic forward dynamic programming (FDP) technique which is well explained in [12]. Since the battery powers are controllable variables, the states I_i ($i=1,\ldots,4$) are defined to include and identify all

possible operating conditions as I_1 = battery is off; I_2 = discharge; I_3 = charge with DG power only; I_4 = charge with DG and/or grid power. Note that in state I_4 charging battery with grid power will increase energy cost at the present time, but the charged energy might discharge later when the energy price is higher. This state is necessary to cover all possible paths reaching optimum result. Although the number of operating states is finite, the value of battery power is determined by satisfying objectives F_1 and F_2. Therefore the value of SOC at each stage can also be any value in continuous domain.

The optimal path is determined by comparing all possible paths from the initial stage to the final stage. The detailed procedure is described as below:

1) For each state I_i^{K+1} at stage $K+1$, find all feasible paths T_{ij} from all states I_j^K in previous stage K.

2) Calculate and select the best path T_{ij} reaching I_i^{K+1}. Where $C(I_i^{K+1})$ is the grid energy cost at state I_i^{K+1}, T_{ij} is transient cost related to on/off action; $F_1(I_j^K)$ is the cumulated cost at previous state.

$$F_1(I_i^{K+1}) = \min\left\{ C(I_i^{K+1}) + T_{ij} + F_1(I_j^K) \right\} \tag{23}$$

3) Go to next stage and repeat from 1). Until final stage.

4) If multiple paths $n=1,...,N$ lead to the same value of F_1, run subroutine to select the path with minimum F_2.

$$F_2(I_i^{K=M}) = \min_{n=1...N}\left\{ \sum_{k=1}^{M} \left(\left\| P_{grid,n}(K) - P_{grid,n} \right\| \right) \right\} \tag{24}$$

IV. DISTRIBUTION LEVEL STATE ESTIMATION

Power system state estimation based on near real-time measurements is used extensively at the transmission level. Generally, the assumed system topology and

SCADA data are combined with redundant measurements and reasonable assumptions based on previous operating points. Note that assumed data points may be derived from solved power flow solutions, historical data, and previously estimated solutions [12]. Again, measurements include real and reactive power injections and flows, bus voltage magnitudes, and relative phase angles where phasor measurements are available. Solution of the estimation procedure provides state estimates where no measurement devices exist.

The state estimation process generally employs non-linear solution methods to iteratively find a least square approximation to an over determined problem. Generally, the non-linear solution employed is similar to the Newton-Raphson technique used for power flow analysis, except for the measurement Jacobian describing the non-linear relation of the states to measurements.

Utilizing near real-time data enhances monitoring, analysis and control of distribution systems. Applications of a distribution class state estimator are discussed in Section IV-A. Three-phase distribution feeder s often have characteristics that preclude transfer of modeling and analysis methods from trans-mission engineering. Such characteristics include unbalanced loading, laterals serving single-phase loads, conductors with high r/x ratios, and small, stochastic, distributed generators. These systems require unique sets of analysis tools and modeling algorithms that adequately capture the range of operating conditions and system characteristics. Distribution power flow studies often utilize a robust ladder iterative technique to solve for bus voltage profiles and current flows for radial systems. A practical distribution system state estimation algorithm is developed.

A. Applications of a Distribution Class Estimator

State estimation may be used to enable control functions in a number of scenarios. For example, comparing estimated flows and voltages to ratings or switching to prevent component overload. A list of potential benefits includes:

- Optimization and generation rescheduling based on forecasted states,

- Enhanced system wide voltage control capability,

- Single phase voltage regulation and VAR control,

- Enabling voltage regulation via local DG,

- Selective networking of primary and secondary systems,

- Facilitate distribution locational marginal pricing,

- Energy storage management and optimization,

- DG location and control – i.e. to relieve congestion, manage prices,

- DMS that provide operators more effective distribution feeder interaction tools; i.e. monitor and visualize the grid, alarms and alerts to operators,

- Enables control signals for demand-side-management,

- Enable demand response that impacts bulk grid operations,

- Fault detection (not protection), isolation, and reconfiguration for enhanced reliability,

- A validation tool –load and topology– for transmission system state estimators.

Knowledge of contemporary system conditions allows operators to push the distribution system closer to its operating limits.

B. Measurement Infrastructure and Synchronized Phasor Measurements in Power System State Estimation

Synchrophasors in state estimation is seen as revolutionary, since system states (bus voltage magnitude and angle) may be directly measured. At the distribution level, synchrophasor measurements may provide three-phase voltage magnitude and angle information to help distribution operators assess unbalance, flows and abnormal operation. This is particularly important, since most conventional distribution operators only have substation SCADA data to gauge feeder condition. Although wide deployment of measurement devices with synchrophasor technology is envisioned, even a few such measurements combined with smart meter data and other measurements may enhance the feasibility of distribution class estimators.

C. Conventional State Estimation Formulation

The process of state estimation in transmission system involves the use of measurements along with a mathematical system representation to obtain least squares fit of estimates to the assumed topology. General assumptions that allow the use of positive sequence equivalent circuit models to estimate the positive sequence states include:

- System topology is known (or processed to within an acceptable limit),

- Balanced three-phase loads,

- Fully transposed lines,

- Symmetrical series or shunt devices on all phases,

State estimation uses a large number of redundant measurements. Where an insufficient set of measurement data exists, historical data (i.e., pseudo-measurements) or virtual measurements (i.e., zero injections) may be substituted to obtain an observable/non-singular process matrix. States may be represented as polar or rectangular

quantities. At a given operating point, the non-linear relationship of measurements to states is given by (25),

$$h(x) = z \tag{25}$$

where z is a vector of measurements, x is the vector of system states (bus voltage magnitude and angle), and h is a non-linear vector valued function that relates system states to corresponding measurements. Typically the power system state estimation problem presents itself as an over determined system where redundant measurements outnumber states.

Weighted least squares estimation involves the minimization of the 2-norm of the residual vector denoted by r,

$$r = z - h(x) \tag{26}$$

The 2-norm of the residual vector is the non-linear objective function, a scalar, $J(x)$,

$$J(x) = \sum_{k=1}^{n} \left(z_k - h_k(x) \right)^2 = r^t r \tag{27}$$

where k is an arbitrary bus number and n is the number of measurements. The solution is found at the simultaneous minimization of each measurement residual,

$$\min \quad J(x) = \frac{\partial \left[\sum_{k=1}^{n} (z_k - h_k(x))^2 \right]}{\partial x} = \frac{\partial r^t r}{\partial x} = 0 \tag{28}$$

At the operating point, $h(x)$ may be linearized around x; and the solution at this point may be expressed linearly,

$$hx = z \tag{29}$$

The solution to the system of equations may be calculated at,

$$x = [h^t h]^{-1} h^t z \tag{30}$$

References [12], [13] provide further discussion on weighted least squares estimation and the gain matrix.

D. *A Three-Phase, Linear Distribution System State Estimator Using Synchronized Phasor Measurements*

The three-phase, untransposed distribution system requires a different set of tools capable of estimating all phase voltage in-formation. The formulation developed in [14] utilizes complex rectangular synchronized phasor measurements and mathematical representation of state estimation equations. Note that in the case where synchronized phasor measurement devices are utilized, it is possible to obtain real and imaginary components of measured quantities. Denoting quantities as complex rectangular, variables may be written as $h = h_r + jh_{im}$, $z = z_r + j z_{im}$, $x = x_r + jx_{im}$. Each matrix or vector may be partitioned into real and imaginary subsets denoted by the subscripts r and im respectively.

The residual vector may be separated into its respective real and imaginary parts. The 2-norm may be calculated as shown.

$$\begin{bmatrix} r_r \\ r_{im} \end{bmatrix} = \begin{bmatrix} \left(z_r - h_r x_r + h_{im} x_{im} \right) \\ \left(z_{im} - h_r x_{im} - h_{im} x_r \right) \end{bmatrix} \tag{31}$$

The solution for the estimation of state variables, x, when variables are in rectangular form,

$$\begin{bmatrix} x_r \\ x_{im} \end{bmatrix} = \begin{bmatrix} h_r & -h_{im} \\ h_{im} & h_r \end{bmatrix}^{+} \begin{bmatrix} z_r \\ z_{im} \end{bmatrix} \tag{32}$$

Note that x_r and x_{im} are independent of each other. Estimation of sequence values follows the same formulation previously described. Phasor measurement devices measure individual phase values, and calculate positive, negative, or zero sequence components.

The untransposed line segments with high *r/x* ratio are modeled with an *n_ph* square matrix, where *n_ph* is the number of phases. Four-wire segments are reduced to a 3x3 block matrix using Kron reduction by assuming neutral conductors are solidly grounded at every node. For example, line segment impedance (effective line-ground after Kron reduction for 4-wire) matrix between buses *n* and *m* is,

$$Z_{nm}^{abc} = \begin{bmatrix} Z_{aa} & Z_{ab} & Z_{ac} \\ Z_{ba} & Z_{bb} & Z_{bc} \\ Z_{ca} & Z_{cb} & Z_{cc} \end{bmatrix}_{nm} \tag{33}$$

Where a single or two phase lateral is present, the row and column of the missing phases are zeroed, and the corresponding voltage vector entries in V_{bus}^{abc} are zero. More details of three-phase line, transformer and other device models may be found in [15]. The entries in estimator *h*, *z* and *r* matrices are three-phase (block impedances or voltage and current vectors). The solution vector is three-phase (*a, b, c*).

V. TEST BED SIMULATION AND RESULTS

A. Control Architecture

In the envisioned future distribution system, distributed PV generation and battery storage are installed at end users through solid state controllers. The implementation of active control for distributed resources at customer end is a key element of an automated novel system. The control architecture integrating the algorithms in Sections III and IV is illustrated in Fig. 1. It contains two layers of control on different time frames. The first layer is a day-ahead control including optimization of generation dispatch and energy storage management based on load and generation forecasts. The load demand and PV generation profile for individual customers is derived as forecast input at the beginning of the process and assumed constant during each time interval. The generation dispatch is

first determined for 24 hours without considering battery operations. The DLMPs are calculated for all nodes via OPF process. Then each energy storage unit is optimally scheduled using the hourly DLMPs at its load node. Afterwards, it is necessary to perform OPF with updated net demand taking all storage schedules. In this study, the batteries are reasonably sized so that their operations will not significantly change the net demand and the corresponding DLMPs during each calculation iteration. Therefore a convergence to the final schedule can be assumed when the mismatch of system operations in two consecutive iterations is smaller than the tolerance.

The second layer is a near real-time control based on a distribution level state estimation. The state estimator will continuously take measurements from limited number of sensors or other signal sources (e.g., SCADA) and return the estimated full system status. If a system variable value change or system topology change is detected, proper control actions will be carried out based on the estimated status and DLMPs. Also the system changes will be forwarded to update input information for the next day-ahead schedule.

This control scheme is supposed to provide multiple benefits of higher energy efficiency, minimizing customer energy bill and more reliable control.
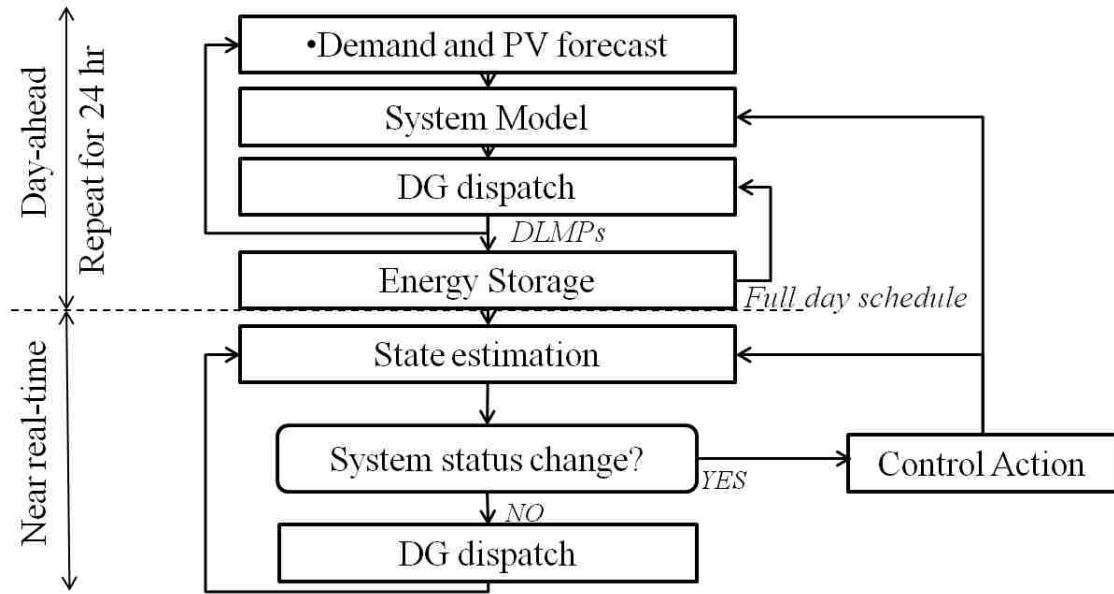
Fig. 1 Proposed control architecture.

B. Test Bed Description

The proposed control algorithms in Sections III and IV have been implemented in a sample distribution system known as the Bus 3 of the Roy Billinton Test System (RBTS) [16]. This distribution system was designed as a balanced 3 phase system including 8 feeders and a total 85MW peak load with various sizes of residential, commercial and industrial loads. Fig. 2 shows the one line diagram, the state estimator measurements are installed at nodes marked by "*." The radius type structure can switch to loop type by closing the breakers at the end of each pair of feeders. The node classifications and configurations are given in TABLE I. The total PV installation capacity is larger than the total peak load. A fully charged battery can discharge for up to 4 hours at maximum power. The day-ahead demand forecast profiles are real demand records obtained from ERCOT, and PV generation is estimated based on local measurement in Missouri under diverse weather conditions.
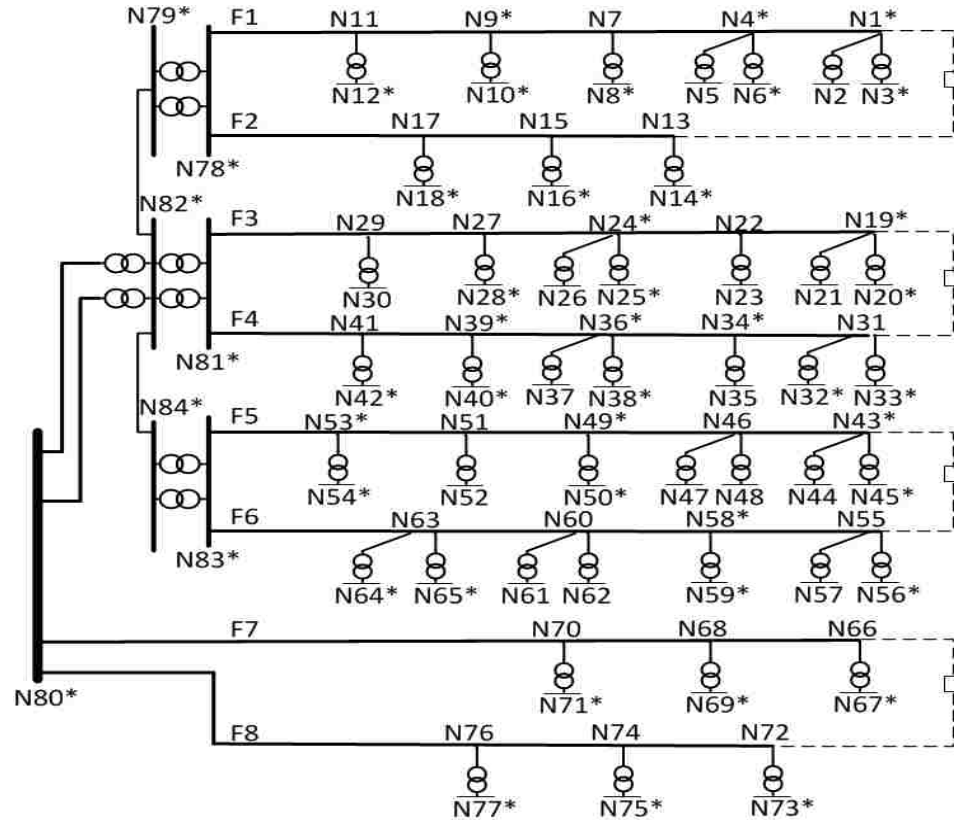
Fig. 2 Distribution system one-line diagram.

TABLE I
SYSTEM CONFIGURATION AND LOADS AND PVS CLASSIFICATION

	Load type	1	2	3
Residential	Load nodes	3, 26, 45, 52	2, 6, 8, 10, 12, 35, 37, 38 40, 42, 56, 57, 59, 61, 62	20, 21, 23, 32, 44
	Peak load (MW)	0.7750	0.8367	0.8500
	PV capacity(MW)	0.950	1.250	1.150
	Battery Pwr.(MW)	0.19	0.25	0.23
Commercial	Load nodes	5, 28, 30, 33, 48, 50, 54, 64, 65	-	25, 47
	Peak load (MW)	0.5222	-	0.9250
	PV capacity(MW)	0.7500	-	1.000
	Battery Pwr.(MW)	0.15	-	0.4
Industrial	Load nodes	14, 16, 18	67, 69, 77	71, 73, 75
	Peak load (MW)	1.0167	6.9167	11.5833
	PV capacity (MW)	6.000	8.000	10.000
	Battery Pwr.(MW)	0.25	0.5	0.5

All distributed resources (PV and battery) are owned by customers, but different control principles are assumed for different types of customers. Each residential node contains 190 to 250 individual customers. Customers are allowed to sell extra PV generation back to the grid, but at a much lower price than the purchasing price (e.g., feed-in-tariff). Residential customers are not participating in the retail market.

Commercial and industrial customers are active sellers in the retail electricity market. The PV generation will be sold at customer defined offer prices. As shown in TABLE II, the legacy grid generation cost ($/MWh) is estimated with quadratic coefficients a_0, a_1, and a_2 based on the cost models described in [16]. The selling bids from individual suppliers are reasonably assigned to intuitively create variant piecewise price segments as in a market environment. However, the impact of bidding price mechanism is not the focus of this work.

TABLE II
ENERGY OFFER PRICES FROM GRID AND PRIVATE SUPPLIERS

Grid	$a_2=0.4$	$a_1=75.5$	$a_0=0$	
	50% Capacity	80% Capacity	90% Capacity	100% Capacity
Com1	75	75	80	80
Com3	72	72	72	75
Ind1	65	72	79	84
Ind2	70	73	80	85
Ind3	68	78	79	83

C. *Illustrative Examples*

• Case 1: sensitivity analysis of DLMP.

This study shows the marginal generation shift between the grid and DGs as load level changes from 75% to 125% of peak and DG capacity changes from 50% to 150%.

As shown in Fig. 3, the DLMP changes at all nodes under different combination of settings. The grid becomes the marginal supplier either when demand exceeds the total DG supply, or when the DGs bid too high at their maximum output. In these cases, the DLMPs are set by the grid and DLMPs increase along each feeder as the distance from substation increases. Such loss cost deviation is most significant under the set of highest load level 125% and lowest DG rating 50%, e.g., the MLC at node 12 is 0.5681 $/MWh (0.3497% of MEC), but is 2.2708 $/MWh (1.3724% of MEC) at node 1 at the end of the same feeder. But this phenomenon changes when DGs become the marginal suppliers (e.g., LD75% and DG100%), the DLMPs increase from the center of marginal DG, and the loss cost are very small (maximum at 0.1442 $/MWh) and almost identical along the same feeder.

In the cases with *LD* ≤100% and *DG* ≥ 125%, the actual total DG capacity is oversized more than 40% over the peak load. The DLMPs are always set by DGs as low as 70–75$/MWh, but much of DG available capacity remain un-dispatched.
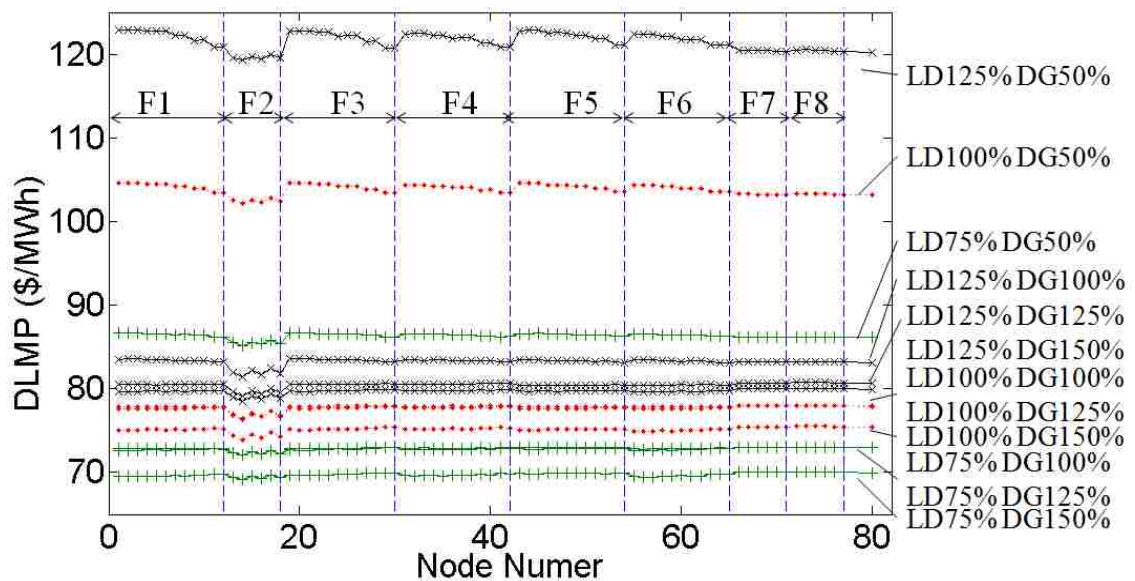
Fig. 3 DLMPs under different load level and DG ratings.

• Case 2: 24-hour day-ahead planning

This case shows the coordinating control of generation dispatch and energy storage management. An hourly optimal power flow is firstly performed in order to get a dispatch result as well as DLMPs at all nodes. Then, these pricing signals are used for energy storage optimization at residential nodes. In practical distribution systems, commercial and industrial load demands are usually higher at daytime and lower at night, which has an approximate match with PV generations. The residential loads however behave in the opposite way. This mismatch shift plus the load level variation (0.3 p.u. to 1.0 p.u.) imply that an optimal loading of generations and coordination with energy storage is necessary.

As the simulation results show in Fig. 4 and Table III, a total of about 6.9 MWh PV energy was wasted (between 11 A.M. and 2 P.M.) if operating without energy storage because some PV generations are out-bid by grid power. With active battery energy management, a total of about 4.4 MWh is used to charge local batteries coupled at PV sites, and then discharged between 8 P.M. to 9 P.M. as DG capacity. The residential battery charge totals 14.6 MWh between 9 A.M. to 2 P.M. Part of this charge is derived from the "wasted" PV energy, and the rest is charged by residential PV generations and grid power. Such operations cause a small in-crease in DLMPs during the day time, but this energy discharge between 7 P.M. and 10 P.M. and brings down the peak DL MP from 141.659 to 136.523 $/MWh.
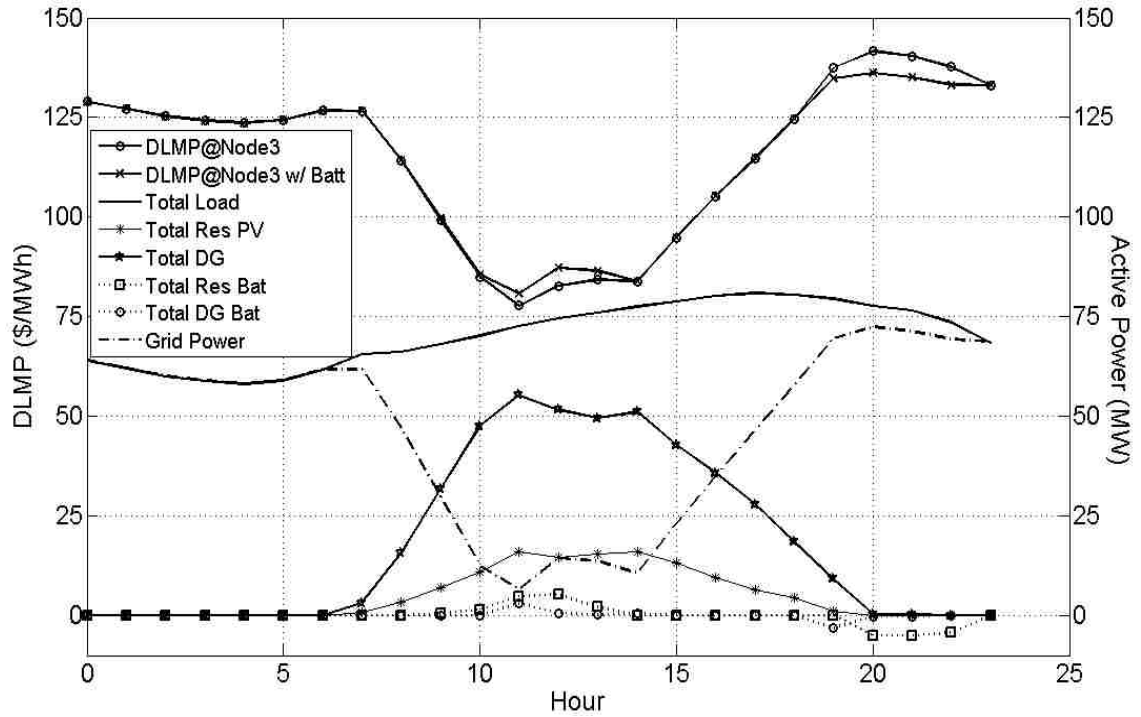
Fig. 4 Day-ahead DG and battery control with sample DLMP at node 3.

TABLE III
RESULTS OF CASE 2 RELATED TO ENERGY EFFICIENCY AND BENEFITS

	no storage	with storage
Wasted PV energy (MWh)	6.884	0
Max DLMP ($/MWh)	141.66 at 8pm	136.52 at 8pm
Min DLMP ($/MWh)	77.033 at 11am	79.7647
Grid energy usage (MWh)	1140.8	1134.6
Daily energy loss (MWh)	2.7403	2.5476

• Case 3: Three-phase simulation and state estimation

In this study case, three phase detailed model is retained to test the state estimator and the loads, primaries, and laterals may be single or three phase. Load and DG configurations are given in Table IV. Feeder diagram is illustrated in Fig. 5.

For this illustration, the DG power factor is varied by changing the set-point of the unit to absorb VARs. The target value of bus 45 phase *C* voltage magnitude is 1.0 p.u. To obtain this, reactive power is absorbed by the generator at 30 kVAr/phase and 40 kVAr/phase. The results are plotted in Fig. 6. Bus voltage on phase C is reduced to 1.0 p.u. when 40 kVAr/phase is absorbed by the distributed generator. This equates to a DG power factor of 0.993 leading.

TABLE IV
LOAD AND DG CONFIGURATIONS FOR CASE 3

Node	Ph.A	Ph.B	Ph.C	Ph.A	Ph.B	Ph.C
		(MW)			(MVar)	
1	0.09	0.10	0.10	0.03	0.03	0.03
2	0.15	0.16	0.00	0.04	0.04	0.00
3	0.00	0.00	0.10	0.00	0.00	0.04
4	0.00	0.09	0.00	0.00	0.04	0.00
5	0.00	0.00	0.12	0.00	0.00	0.03
6	0.12	0.13	0.11	0.04	0.04	0.06
7	0.10	0.00	0.00	0.03	0.00	0.00
DG1	0.33	0.33	0.33			
DG2	0.33	0.33	0.33			
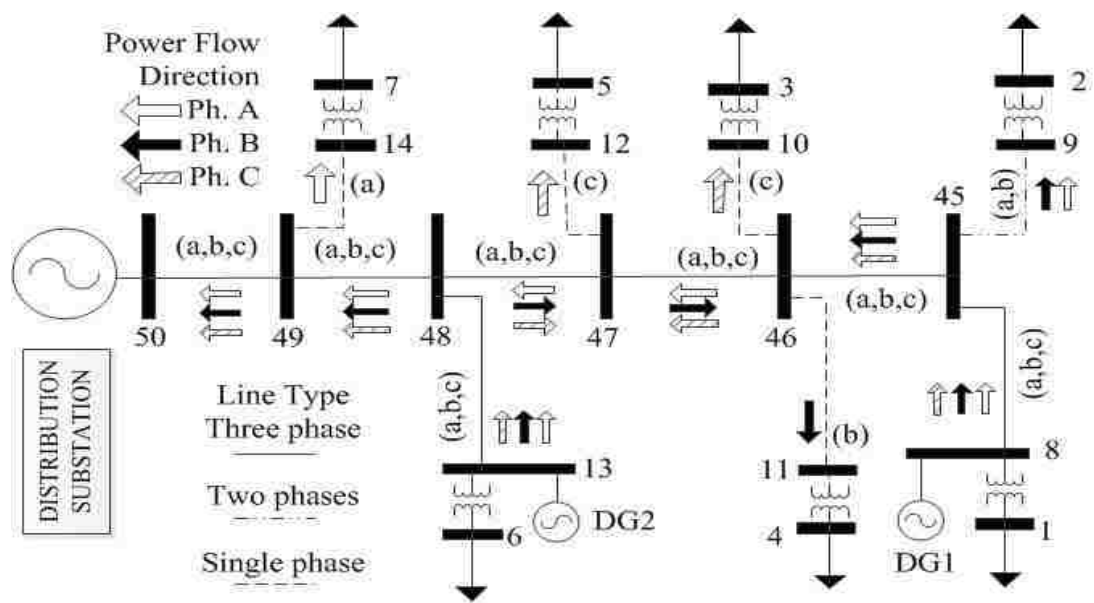
Fig. 5 Feeder F1 developed in 3-phase detail.
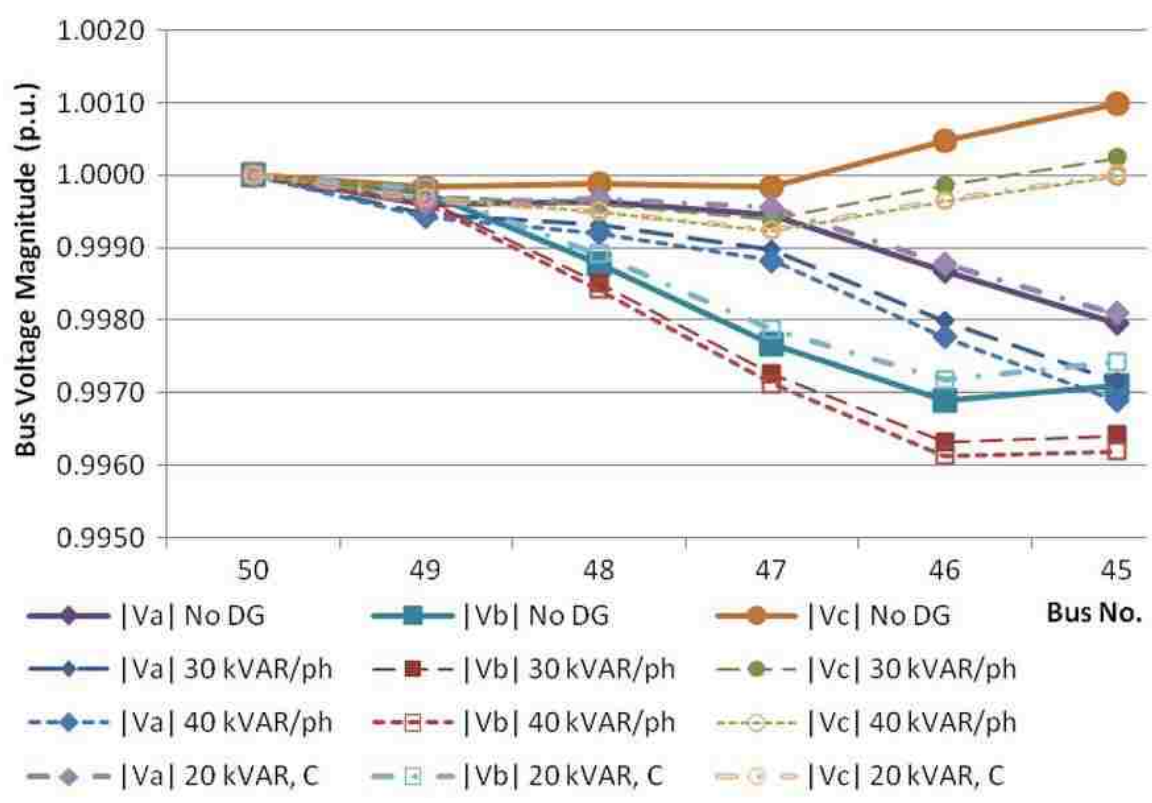
Fig. 6 Bus voltage profile for the loading condition of RBTS feeder F1.

VI. CONCLUSION

The demand expansion and increasing penetration from distributed resource in modern distribution systems necessitate the development of new control method to operate and optimize distributed resources. In this paper, a control method is introduced using pricing index DLMP as a control signal to schedule day-ahead generation dispatch and energy storage management. The proposed control methods fit for distributed resources optimization in an energy retail market environment. Coordination between DG and energy storage shows benefits of energy cost reduction and renewable energy efficiency improvement. The distribution level state estimation enables near real-time control addressing unexpected system status changes.

REFERENCES

[1] Grid 2030: A National Vision for Electricity's Second 100 Years Jul. 2007, Office of Electric Transmission and Distribution, U.S. Dept. of Energy [Online]. Available: http://en ergy.gov/

[2] International Renewable Energy Agency, Renewable Energy Technologies: Cost Analysis Series, vol. 1, no. 4/5, June 2012.

[3] G.T. Heydt, B.H. Chowdhury, M.L. Crow, D. Haughton, B.D. Kiefer, F. Meng, and B. R. Sathyanarayana, "Pricing and control in the next generation power distributed system," IEEE Trans. Smart Grid , vol. 3, no. 2, pp. 907–914, Jun. 2012.

[4] Solar Energy Industry Association, "U.S. solar market insight" [On-line]. Available: http://www.seia.org/

[5] A.Q. Huang, M.L. Crow, G.T. Heydt, J.P. Zheng, and S.T. Dale, "The future renewable electric energy delivery and management," *Proc. IEEE*, vol. 99, no. 1, pp. 133–148, Jan. 2011.

[6] F. Beck and E. Martinot, "Renewable energy policies and barriers," in Encyclopedia of Energy. London, U.K.: Academic/Elsevier Science, 2004, pp. 365–383.

[7] U.S. D.O.E, "The potential benefits of distributed generation and rate-related issues that may impede their expansion," Feb. 2007.

[8] A. Forsgren, P. E. Gill, and M. H. Wright, "Interior method for non-linear optimization," Rev. Soc. Ind. Appl. Math., vol. 44, no. 4, pp. 525–597, Aug. 2006.

[9] R. D. Zimmerman, C. E. Murillo-Sánchez, and R. J. Thomas, "MATPOWER: Steady-state operations, planning and analysis tools for power systems research and education," IEEE Trans. Power Syst., vol. 26, no. 1, pp. 12–19, Feb. 2011.

[10] T. Orfanogianni and G. Gross, "A general formulation for LMP evaluation," IEEE Trans. Power Syst., vol. 22, no. 3, pp. 1163–1173, Aug. 2007.

[11] J. Eyer and G. Corey, "Energy storage for the electricity grid: Benefits and market potential assessment guide," Sandia National Laboratories, Feb. 2010.

[12] A. J. Wood and B. F. Wollenberg, Power Generation Operation and Control, 2nd ed. New York: Wiley, 1984.

[13] A. Abur and A. G. Exposito, Power System State Estimation—Theory and Implementation. New York: Marcel Dekker, 2004.

[14] D. A. Haughton and G. T. Heydt, "A linear state estimation formulation for smart distribution systems," IEEE Trans. Power Syst., vol. 28, no. 2, pp. 1187–1195, May 2013.

[15] W. H. Kersting , Distribution System Modeling and Analysis .New York: CRC, 2007.

[16] R. Billinton and S. Jonnavithula, "A test system for teaching overall power system reliability assessment," IEEE Trans. Power Syst., vol. 11, no. 4, pp. 1670–1676, Nov. 1996.

[17] U.S. Energy Information Administration, "Annual Energy Outlook 2012." [Online]. Available: http://www.eia.gov/forecasts/aeo

[18] Power System Engineering Research Center, "Implications of the smart grid initiative on distribution engineering", 2014 [Online]. Available: http://www.pserc.wisc.edu/research/public_reports.aspx

II.   A Three-Phase Optimal Power Flow Program for Control and Optimization of Distributed Generations

F. Meng, Student Member, *IEEE*,   B. Chowdhury, Senior Member, *IEEE*

Abstract – **The ever-increasing penetration of distributed generation (DG) in recent years brings challenges as well as opportunities for distribution companies to evolve into the smart grid paradigm. A new three-phase unbalanced optimal power flow (OPF) program has been developed for steady state system analysis to minimize the cost of serving loads in a distribution network. The algorithm is developed based on primal-dual interior point method (PDIPM). Comprehensive system components and constraints are modeled in a generalized fashion. In tests performed on the IEEE test feeder systems, the proposed algorithm is able to solve for optimal solutions under various system conditions and constraints. The potential applications of the program for distribution system design, reconfiguration, and control are also highlighted.**

Index Terms— **Unbalanced system; optimization; primal-dual interior point method; distributed energy resource; current injection method; power balance method.**

I. INTRODUCTION

Power system infrastructures and operations in the U.S., Europe and several other parts of the world have gradually transformed from regulated monopolies into a competitive market-based environment since the evolutionary industry restructuring

efforts of the early 1990's [1]. While drastic changes have taken place at the transmission and sub-transmission levels, the lower voltage distribution system has remained essentially unchanged, especially in aspects of operation and control [2]. Recently though, the smart grid (SG) concept promises economic and environmental benefits as well as higher efficiency for the future power delivery system [3]-[5]. Many structural modifications and efforts are underway in distribution systems to evolve into a smart grid operating environment. In France, for example, independent distribution network operators (DNO) have been formed to optimize the energy supply at the substation, including small energy suppliers within distribution networks, in order to serve customers at optimum levels of economics and reliability [6]. Some utilities in the U.S. are endeavoring to overcome technology and regulatory issues to build a smart and agile distribution network where customers can generate and share electricity [7].

In this paper, the authors envision a distribution network featuring elements of novel SG infrastructure and an entity similar to a DNO who is responsible for optimally operating the distribution system in a secure manner and at least cost. We assume that the distribution system of the future will include a large proportion of Distributed Generation (DG) that operate in parallel with conventional generation available at the main substations. DGs are small power generation units (below 1 MW) located near or on site of customers in a distribution network. In addition to the environmental benefits, especially from renewable DGs, the overall energy cost of transmission and distribution (T&D) may be lowered by integrating DGs. Customers may also receive financial benefits from utility pricing programs (e.g. net-metering, feed-in-tariffs, etc.). While the average capital cost keeps decreasing, DGs have become a more promising alternative

source other than transmission supplier for both utility and consumers. The total installation of DGs, especially renewable, has shown a rapid growth in recent years [8].

While the placement of smart meters is one of the fundamental changes occurring at the distribution level, more importantly, digitalization and data communication are starting to become more common features of the smart distribution network. With instant signal feed and communication directly with the customer, it is possible for the DNO to execute more complicated analysis and optimization on the new digitalized platform [4].

Advanced power electronic devices are also playing more important roles in the distribution network, particularly for distributed resource integration, power quality improvement, and even protection.

Notwithstanding the numerous benefits these new technologies can potentially provide, one cannot ignore the fact that the underlying physical distribution system has essentially remained the same since when most of it was built decades ago − as a combination of single, double, and three-phase lines pulled along with a neutral wire and designed as a radial system. High penetrations of customer-owned DG can best be dispatched in a non-discriminatory manner by the DNO who can optimally aggregate the profitability from the distributed resources while maintaining the security level of the system. With this backdrop, an unbalanced three-phase OPF is proposed in this paper to solve such problems based on three-phase power flow analysis and non-linear optimization using the primal-dual interior point method (PDIPM).

A classic Newton-Raphson algorithm for three-phase load flow considering the nodal power balance method (PBM) was presented early in 1974 [9]. Later, the current injection method (CIM) was introduced [10]. Both PBM and CIM are considered for OPF

formulation in this paper. The basic system component models were developed for load, transformer, voltage regulator, etc., in [11].

PDIPM is a suitable and widely-adopted method for non-linear optimization problems. The mathematic theories about PDIPM can usually be found in applied mathematics publications [12]. Its application in unbalanced three-phase system is relatively new. Some recent research work have been presented with different optimization objectives such as voltage unbalancing control [13], loss reduction and load curtailment [14], etc.

The OPF algorithm proposed in this paper is a generalized program to minimize the total generation cost for the DNO to serve all loads in the system while maintaining the stated security constraints (voltage and line loading). Some features of the proposed algorithm include:

- capability to solve for general distribution systems with various component configuration and structure (radial or looped);

- capability to solve for optimal DG operation to maximize economic benefits within security limits;

- derivation of marginal generation and nodal shadow price from the solution, which are useful for extended analysis such as optimal system design and planning;

- adaptation of two alternative methods - PBM and CIM - to solve the OPF problem.

II. BASIC MODELS IN DISTRIBUTION SYSTEMS

Distribution systems tend to have many more complex components and devices as compared to transmission systems. There elements must be modeled in detail in order to obtain accurate and reliable results from an analysis. This section introduces the comprehensive models of components and devices that are commonly used in distribution systems. These models are categorized as nodal injection elements and branch elements.

A. Nodal Injection Elements

- Load

Loads in a distribution system are typically specified by the average maximum complex power demand. The types of loads are summarized in TABLE I based on connection and demand types. For simplification purpose, the distributed loads are converted to lumped loads with portion factors *a* and *1-a* ($0 \leq a \leq 1$) at both ends of the line segment.

Most loads can be characterized as constant impedance, current, and/or power (also known as ZIP load). The effective demand of the ZIP load is a function of the nodal voltage magnitude, and this feature has been taken into account in the OPF algorithm. Shunt capacitor banks are commonly used to provide reactive power support and can be treated as a special constant power load given in kVar.

TABLE I
TYPICAL TYPES OF LOADS IN DISTRIBUTION SYSTEM

Connection	Spot Load		Distributed Load
	Wye		Delta
Demand Type	Constant PQ	Constant I	Constant Z

- Distributed generation

All DGs are modeled as controllable power sources with a linear limit on generation capacity. Each generation can have either a quadratic or a piecewise linear cost function, which is presented in Section III.A.

B. *Branch Elements*

- Conductors

The overhead line, underground cable or other conductors in a distribution system are modeled using the π-model (Fig. 1). Since the conductors usually consist of single-phase, two-phase, and three-phase segments, the untransposed model is adopted to retain the self and mutual impedance correctly. Given the conductor characteristics, the three-wire equivalent impedance matrix can be calculated using the well-known Carson's equation [11]. The admittance matrix of branch element is given in (1).

$$\begin{bmatrix} I^a \\ I^b \\ I^c \end{bmatrix} = \begin{bmatrix} & & \\ & Y_{bus} & \\ & & \end{bmatrix} \cdot \begin{bmatrix} V_i^a - V_j^a \\ V_i^b - V_j^b \\ V_i^c - V_j^c \end{bmatrix} \tag{1}$$
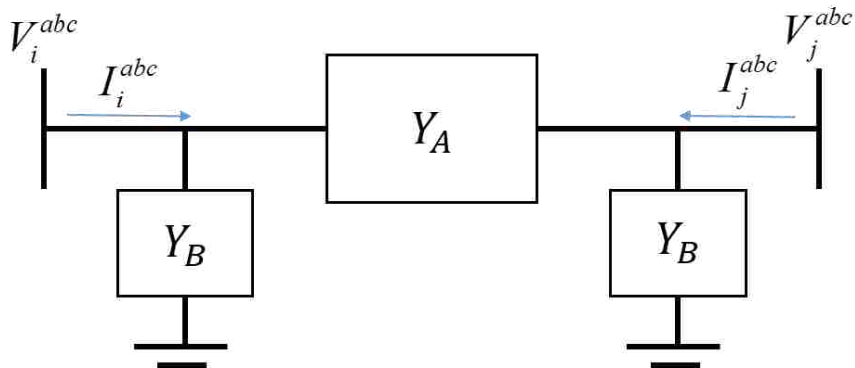
Fig. 1 The π-Model of Conductors.

- Transformer

Three-phase transformers are commonly used to convert voltage levels at substation or at the customer's end. There are various types of connections and the general format of the admittance matrix, considering tap changing ratio and angle shift, is given in (2). The general admittance matrices of common connection types are given in Table II. The general diagram of three-phase transformer admittance matrix is illustrated in Fig. 2.

$$
\begin{bmatrix} I^P_{abc} \\ \cdots \\ I^S_{abc} \end{bmatrix} = \begin{bmatrix} Y^{PP} & \vdots & Y^{PS} \\ \cdots & \cdots & \cdots \\ Y^{SP} & \vdots & Y^{SS} \end{bmatrix} \begin{bmatrix} V^P_{abc} \\ \cdots \\ V^S_{abc} \end{bmatrix}
\tag{2}
$$

Table II
THREE-PHASE TRANSFORMER ADMITTANCE SUB MATRICES FOR COMMON CONNECTIONS

Connection		Self admittance		Mutual admittance	
Primary	Secondary	Y_T^{PP}	Y_T^{SS}	Y_T^{PS}	Y_T^{SP}
Wye-Grounded	Wye-Grounded	$C_I \dfrac{y_T}{a_T^* a_T}$	$C_I y_T$	$-C_I \dfrac{y_T}{a_T^*}$	$-C_I \dfrac{y_T}{a_T}$
Delta	Delta	$C_{II} \dfrac{y_T}{a_T^* a_T}$	$C_I y_T$	$C_{III}^T \dfrac{y_T}{a_T^*}$	$C_{III} \dfrac{y_T}{a_T}$
Delta	Wye-Grounded	$C_{II} \dfrac{y_T}{a_T^* a_T}$	$C_{II} y_T$	$-C_{II} \dfrac{y_T}{a_T^*}$	$-C_{II} \dfrac{y_T}{a_T}$

C_I, C_{II}, and C_{III} are transforming matrices

$$
C_I = \begin{bmatrix} 1 & 0 & 0 \\ 0 & 1 & 0 \\ 0 & 0 & 1 \end{bmatrix}, C_{II} = \frac{1}{3} \cdot \begin{bmatrix} 2 & -1 & -1 \\ -1 & 2 & -1 \\ -1 & -1 & 2 \end{bmatrix}, C_{III} = \frac{1}{\sqrt{3}} \cdot \begin{bmatrix} -1 & 1 & 0 \\ 0 & -1 & 1 \\ 1 & 0 & -1 \end{bmatrix}
$$

y_T is the three phase leakage impedance matrix

$$
y_T = \begin{bmatrix} y_{T,a} & 0 & 0 \\ 0 & y_{T,b} & 0 \\ 0 & 0 & y_{T,c} \end{bmatrix}
$$

a_T is the three phase voltage ratio matrix with angle shift $a_{T,abc} = \alpha_{abc} \angle \beta_{abc}°$

$$a_T = \begin{bmatrix} a_{T,a} & 0 & 0 \\ 0 & a_{T,b} & 0 \\ 0 & 0 & a_{T,c} \end{bmatrix}$$
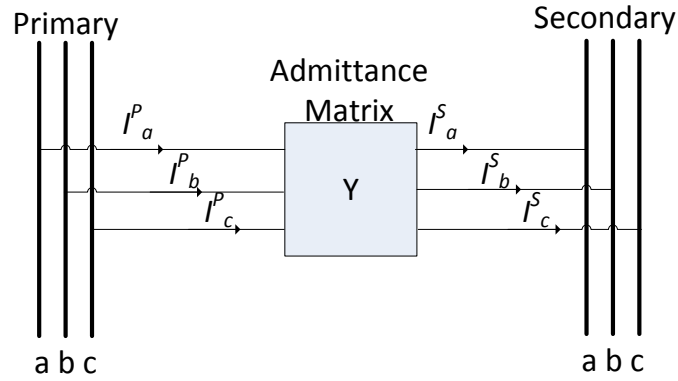
Fig. 2 General diagram of three-phase transformer.

- Voltage Regulator

Voltage regulators are important devices to regulate voltage at the substation bus or to compensate voltage drop along the main primary feeder segments by changing the tap positions. Regulators can be categorized as type-A and type-B, which can be modeled as special tap changing autotransformer. Therefore the general formulation of the admittance matrix can also be expressed as in (2), and the equivalent voltage ratios is found in TABLE III.

TABLE III
EQUIVALENT VOLTAGE CHANGE RATIOS OF TYPE-A AND TYPE-B VOLTAGE REGULATORS

Tap Changing Location	Type A	Type B
Primary Side	$a_{T,abc} = 1 - 0.00625 \cdot Tap_{abc}$	$a_{T,abc} = 1 + 0.00625 \cdot Tap_{abc}$
Secondary Side	$a_{T,abc} = \dfrac{1}{1 - 0.00625 \cdot Tap_{abc}}$	$a_{T,abc} = \dfrac{1}{1 + 0.00625 \cdot Tap_{abc}}$

$Tap_{abc} = +/- 1, 2, \ldots, 16$

III. THREE-PHASE UNBALANCED OPF ALGORITHM

This section describes the OPF formulation based on PDIPM. The generalized formulation of the non-linear optimization problem with equality and inequality constraints is defined by (3) - (6). In this study, the objective function of the OPF is to minimize the total generation costs from substation and distributed energy resources. The cost function of each power supplier can be either polynomial non-linear or piecewise linear format.

A. Generalized OPF Problem

The optimization problem is to minimize the total generation cost to serve all demands while satisfying variable limits as well as nodal power/current balance and line flow limits.

$$\min \quad F(x) = \sum_{i \in polynomial} f_i(x) + \sum_{j \in piecewise} f_j(x) \tag{3}$$

s.t.

$$x = \begin{bmatrix} x_1 & x_2 \mid x_3 & x_4 \mid x_5 \end{bmatrix} = \begin{bmatrix} V_{mag} & V_{ang} \mid Pg & Qg \mid x_{pw} \end{bmatrix}^T$$
$$or \tag{4}$$
$$x = \begin{bmatrix} x_1 & x_2 \mid x_3 & x_4 \mid x_5 \end{bmatrix} = \begin{bmatrix} V_R & V_M \mid Pg & Qg \mid x_{pw} \end{bmatrix}^T$$

$$G(x) = \begin{bmatrix} G_{NLN}(x) \\ \hline G_{LN}(x) \end{bmatrix} = 0 \tag{5}$$

$$H(x) = \begin{bmatrix} H_{NLN}(x) \\ \hline H_{LN}(x) \end{bmatrix} \leq 0 \tag{6}$$

Where

x is a vector of independent variables. x_1 and x_2 are three-phase nodal voltage magnitude and angle in the PBM algorithm, or nodal voltage real and imaginary components in the CIM algorithm. x_3 and x_4 are controllable three-phase active and reactive generation power. x_5 is an additional helper variable corresponding to three-phase piecewise generation costs.

$F(x)$ is the objective function as the summation of polynomial and piecewise generation costs.

$G(x)$ and $H(x)$ are vectors of equality and inequality constraints containing both non-linear (G_{NLN} and H_{NLN}) and linear (G_{LN} and H_{LN}) parts, respectively.

B. Cost Functions

For each electricity supplier, the generation cost is defined as the dollar value to supply electricity at a specific power in a specific time interval, given in $/hour. The function for each electricity supplier can be either non-linear polynomial or linear piecewise. Only the active power cost is considered in this study.

$$F(x) = \min\left(\sum f_{poly}(x) + \sum f_{pw}(x) \right) \tag{7}$$

The first and second order derivatives of cost function are generalized as:

$$\nabla F = \nabla f_{poly} + \nabla f_{pw} \tag{8}$$

$$\nabla^2 F = \nabla^2 f_{poly} + \nabla^2 f_{pw} \tag{9}$$

a) Polynomial cost function

For each generation with polynomial cost ($/h), the cost and the derivatives are given as:

$$f_{poly}(x) = a_{0,j} + a_{1,j} \cdot Pg_j + a_2 \cdot Pg_j^2 \tag{10}$$

$$\nabla f_{poly}(x) = a_{1,j} + 2a_{2,j} \cdot Pg_j \tag{11}$$

$$\nabla^2 f_{poly}(x) = 2a_{2,j} \tag{12}$$

Where

j= 1, 2, …, n is sequence of generations with polynomial cost functions.

a_0, a_1 and a_2 are polynomial factors.

b) Piecewise linear cost function

Piecewise linear costs are usually given as linear segments of constant energy bids y_{pw} ($/MWh) within specific generation range (MW), as illustrated in Fig. 3 (a). These

discontinuous segments can be converted into a continuous linear cost function f_{pw} [22], shown in Fig. 3 (b) and as given in (13). f_{pw} is used for cost function calculation given in unit of ($/h).

$$f_{pw}(x) = price_{j,i} \cdot (Pg_j - P_{j,i}) + C_{pwj,i} \quad , \quad P_{j,i-1} \le Pg_j \le P_{j,i} \quad (13)$$

where

$j = 1, 2, …, n$, is the sequence of generations with piecewise cost function.

$i = 1, 2, …, m$, is sequence of price segments.

C_{pw} is cumulative cost.

Since the partial derivatives of f_{pw} can only be evaluated in discontinuous segments, a constrained helper variable x_{pw} is created equal to f_{pw}. This variable is added to the independent variable x vector as shown in (4). The dimension of x_{pw} is the total number of generations with piecewise cost function. The derivatives of f_{pw} will only consider x_{pw} since Pg is already included in x_{pw}.

$$\nabla f_{pw}(x) = \partial f_{pw} / \partial x_{pwj} = 1 \quad (14)$$
$$\nabla^2 f_{pw}(x) = 0 \quad (15)$$

The linear constraints for x_{pw} can be expressed in a linear matrix format associated with Pg as:

$$\begin{bmatrix} price_{i,j} & -1 \end{bmatrix} \cdot \begin{bmatrix} Pg_j \\ x_{pw,j} \end{bmatrix} \le \begin{bmatrix} price_{i,j} \cdot P_{i,j} - C_{pwi,j} \end{bmatrix} \quad (16)$$
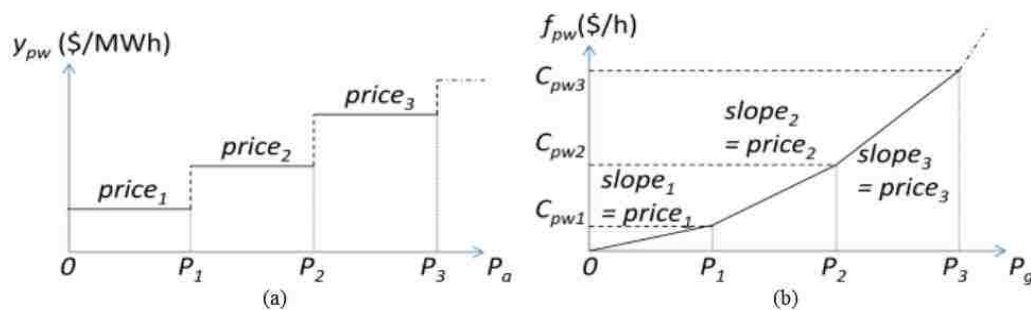
Fig. 3 Piecewise cost segments y_{pw} and constrained variable f_{pw}.

C. Constraints in PBM and CIM

Two alternative methods – PBM and CIM – are adopted to evaluate the equality and inequality constraints G and H, and their derivatives.

a) PBM

In the PBM, the primal independent variables x are defined as:

$$x = [\underset{x_1}{V_{mag}} \quad \underset{x_2}{V_{ang}} \quad \underset{x_3}{Pg} \quad \underset{x_4}{Qg} \quad \underset{x_5}{x_{PW}}] \tag{17}$$

The non-linear G considers nodal active and reactive power balance:

$$G_{NLN} = \begin{bmatrix} G^P \\ G^Q \end{bmatrix} = \begin{bmatrix} P_i^{CAL} - \left(Pg_i - Pd_i \right) \\ Q_i^{CAL} - \left(Qg_i - Qd_i \right) \end{bmatrix} \begin{matrix} \leftrightarrow \lambda_P \\ \leftrightarrow \lambda_Q \end{matrix} \tag{18}$$

$$V_i \left(I_i^{CAL} \right)^* = S_i^{CAL} = V_i \left(Y_{BUS} V_i \right)^* = P_i^{CAL} + jQ_i^{CAL} \tag{19}$$

where

λ_P and λ_Q are the dual variables in Lagrange function.

Y_{BUS} is the nodal admittance matrix.

P^{CAL} and Q^{CAL} are summation of three-phase nodal power injections from all connecting branches at node i.

$P_{g,i}$, $Q_{g,i}$, $P_{d,i}$ and $Q_{d,i}$ are nodal power injections at node i contributed from generation and demand. Note that the demands are the equivalent power consumption of the ZIP load under specific phase voltage magnitudes, which can be expressed as:

$$Sd_i = Pd_i + jQd_i = Sd_i^{PQ} + Sd_i^I V_{mag,i} + Sd_i^Z V_{mag,i}^2 \tag{20}$$

The non-linear H considers the squared complex line flow limits at both *from* and *to* ends of each line.

$$H_{NLN} = \begin{bmatrix} H^f \\ \hdashline H^t \end{bmatrix} = \begin{bmatrix} \left(S_j^f \right)^2 - \left(S_{\max j}^{\,f} \right)^2 \\ \hdashline \left(S_j^t \right)^2 - \left(S_{\max j}^{\,t} \right)^2 \end{bmatrix} \begin{matrix} \leftrightarrow \mu^f \\ \leftrightarrow \mu^t \end{matrix} \tag{21}$$

$$S^f = P^f + jQ^f = V_j^f \left(I_j^f \right)^* = V_j^f \left(Y_{BUS}^f V_i \right)^* \tag{22}$$

$$S^t = P^t + jQ^t = V_j^t \left(I_j^t \right)^* = V_j^t \left(Y_{BUS}^t V_i \right)^* \tag{23}$$

Where

μ_f and μ_t are the dual variables in the Lagrange function.

V_j^f and V_j^t are the complex voltages at *from* and *to* ends of branch j.

Y_{BUS}^f and Y_{BUS}^t are branch admittance matrix for *from* and *to* ends respectively.

- Derivative of *G*:

$$\nabla G_{NLN} = \begin{bmatrix} \partial G^P / \partial x \\ \partial G^Q / \partial x \end{bmatrix} = \begin{bmatrix} G_{x_1}^P & G_{x_2}^P & G_{x_3}^P & G_{x_4}^P & G_{x_5}^P \\ G_{x_1}^Q & G_{x_2}^Q & G_{x_3}^Q & G_{x_4}^Q & G_{x_5}^Q \end{bmatrix} \tag{24}$$

- Hessian of *G*:

$$\nabla^2 G_{NLN} (\lambda) = \frac{\partial}{\partial x} \left(G_x^T \cdot \lambda \right) = \frac{\partial}{\partial x} \left(\begin{bmatrix} G_x^P \\ G_x^Q \end{bmatrix}^T \cdot \begin{bmatrix} \lambda_P \\ \lambda_Q \end{bmatrix} \right) \tag{25}$$

- Derivative of *H*:

$$\nabla H_{NLN} = \begin{bmatrix} \partial H^f / \partial x \\ \partial H^t / \partial x \end{bmatrix} = \begin{bmatrix} H_{x_1}^f & H_{x_2}^f & H_{x_3}^f & H_{x_4}^f & H_{x_5}^f \\ H_{x_1}^t & H_{x_2}^t & H_{x_3}^t & H_{x_4}^t & H_{x_5}^t \end{bmatrix} \tag{26}$$

- Hessian of *H*:

$$\nabla^2 H (\mu) = \nabla^2 H_{NLN} (\mu) = \frac{\partial}{\partial x} \left(H_x^T \cdot \mu \right) = \frac{\partial}{\partial x} \left(\begin{bmatrix} H_x^f \\ H_x^t \end{bmatrix}^T \cdot \begin{bmatrix} \mu_f \\ \mu_t \end{bmatrix} \right) \tag{27}$$

b) CIM

In the CIM, the nodal and branch voltage and current elements are represented in real and imaginary rectangular coordinates. The voltage magnitude limits have to be modeled as non-linear equality constrains for all slack and PV nodes if there is any, and non-linear inequality constrains for all PQ nodes.

$$\begin{array}{ccccc} x_1 & x_2 & x_3 & x_4 & x_5 \\ x = [V_R & V_M & Pg & Qg & x_{PW}] \end{array} \tag{28}$$

The admittance matrix Y_{BUS} can be converted into rectangular coordinates format as:

$$
\begin{bmatrix} I_{M,1}^{abc} \\ I_{R,1}^{abc} \\ \vdots \\ I_{M,n}^{abc} \\ I_{R,n}^{abc} \end{bmatrix} = \begin{bmatrix} B_{11}^{abc} & G_{11}^{abc} & \cdots & B_{1n}^{abc} & G_{1n}^{abc} \\ G_{11}^{abc} & -B_{11}^{abc} & & G_{1n}^{abc} & -B_{1n}^{abc} \\ \vdots & & \ddots & & \vdots \\ B_{n1}^{abc} & G_{n1}^{abc} & & B_{nn}^{abc} & G_{nn}^{abc} \\ G_{n1}^{abc} & -B_{n1}^{abc} & \cdots & G_{nn}^{abc} & -B_{nn}^{abc} \end{bmatrix} \cdot \begin{bmatrix} V_{R,1}^{abc} \\ V_{M,1}^{abc} \\ \vdots \\ V_{R,n}^{abc} \\ V_{M,n}^{abc} \end{bmatrix} \tag{29}
$$

Rearranging the order of rows and columns in (29) to obtain a decoupled formulation for the real and imaginary parts as:

$$
\begin{bmatrix} I_R \\ \hline I_M \end{bmatrix} = \begin{bmatrix} Y_{RR} & \vdots & Y_{RM} \\ \hline Y_{MR} & \vdots & Y_{MM} \end{bmatrix} \cdot \begin{bmatrix} V_R \\ \hline V_M \end{bmatrix} \tag{30}
$$

Similarly the branch admittance matrices Y_{BUS}^{f} and Y_{BUS}^{t} can also be re-written in decoupled rectangular format as:

$$
\begin{bmatrix} I_R^{f} \\ \hline I_M^{f} \end{bmatrix} = \begin{bmatrix} Y_{RR}^{f} & \vdots & Y_{RM}^{f} \\ \hline Y_{MR}^{f} & \vdots & Y_{MM}^{f} \end{bmatrix} \cdot \begin{bmatrix} V_R \\ \hline V_M \end{bmatrix} \tag{31}
$$

The formulation for *to* end keeps the same structure with only substituting the superscript *f* with *t*.

In CIM the equality non-linear constraints is nodal current balance as:

$$
G_{NLN} = \begin{bmatrix} G^{R} \\ G^{M} \\ G^{V} \end{bmatrix} = \begin{bmatrix} I_{R,i}^{CAL} - I_{R,i}^{SP} \\ I_{M,i}^{CAL} - I_{M,i}^{SP} \\ V_{R,i}^{2} + V_{M,i}^{2} - V_{max,i}^{2} \end{bmatrix} \begin{array}{l} \leftrightarrow \lambda_R \\ \leftrightarrow \lambda_M \\ \leftrightarrow \lambda_V \end{array} \tag{32}
$$

$$
I_{R,i}^{SP} = \frac{\left(P_{g,i} - P_{d,i}\right) \cdot V_{R,i} + \left(Q_{g,i} - Q_{d,i}\right) \cdot V_{M,i}}{V_{R,i}^{2} + V_{M,i}^{2}} \tag{33}
$$

$$
I_{M,i}^{SP} = \frac{\left(P_{g,i} - P_{d,i}\right) \cdot V_{M,i} - \left(Q_{g,i} - Q_{d,i}\right) \cdot V_{R,i}}{V_{R,i}^{2} + V_{M,i}^{2}} \tag{34}
$$

Where

$I_{R,i}^{CAL}$ and $I_{M,i}^{CAL}$ are calculated nodal currents at node i.

$I_{R,i}^{SP}$ and $I_{R,i}^{SP}$ are net current injections from nodal demand and generation at node i.

An alternative formulation for G_{NLN} can be evaluated by deriving the nodal power balance using rectangular nodal elements. The purpose is to keep the dual variable λ_P and λ_Q as the nodal shadow prices if such information is required.

$$\left[P_i^{CAL}\right]=\left[V_{R,i}^{abc}\right]\cdot\left[I_{R,i}^{abc}\right]+\left[V_{M,i}^{abc}\right]\cdot\left[I_{M,i}^{abc}\right] \tag{35}$$

$$\left[Q_i^{CAL}\right]=\left[V_{M,i}^{abc}\right]\cdot\left[I_{R,i}^{abc}\right]-\left[V_{R,i}^{abc}\right]\cdot\left[I_{M,i}^{abc}\right] \tag{36}$$

The inequality non-linear constraints H_{NLN} contains the same squared branch flow limits as in (21), with additional voltage limits for PQ nodes as:

$$\begin{aligned} H^{V+} &= V_{R,i}^2 + V_{M,i}^2 - V_{max,i}^2 &&\leftrightarrow \mu_{V+}\\ H^{V-} &= -(V_{R,i}^2 + V_{M,i}^2)+V_{min,i}^2 &&\leftrightarrow \mu_{V-}\end{aligned} \tag{37}$$

The derivatives of G and H in CIM can be derived in a similar procedure as in (24) through (27).

D. Lagrange Function

The Lagrange function L is created based on Eqs. (3) through (6)

$$L(x,\lambda,\mu,z)= F(x)+\lambda^T\cdot G(x)+\mu^T\cdot\left(H(x)+z\right)-\gamma\cdot\sum\ln(z) \tag{38}$$

Where

λ and μ are vectors of dual variables assigned to $G(x)$ and $H(x)$ respectively. The dual variables keep the same dimensions as their corresponding constrains.

$z>0$ is a vector of primal slack variable with the same dimension of $H(x)$.

$\gamma>0$ is a barrier parameter.

E. *Optimality Conditions*

First order partial derivatives of the Lagrange function are given as:

$$\nabla L_{x,\lambda,\mu,z} = \begin{bmatrix} L_x \\ L_\lambda \\ L_\mu \\ L_z \end{bmatrix} = \begin{bmatrix} F_x + G_x^T \cdot \lambda + H_x^T \cdot \mu \\ G(x)^T \\ H(x)^T + z^T \\ \mu^T - \gamma \cdot \sum (1/z) \end{bmatrix} \tag{39}$$

According to [12], the Karush-Kuhn-Tucker (KKT) optimality conditions for the OPF problem are satisfied when

1. The first order derivatives of the Lagrange function $\nabla L_{x,\lambda,\mu,z}$ are all equal to zero.

2. The barrier constant γ tends to zero.

Given $z>0$ such optimality conditions are modified as:

$$\nabla L_{x,\lambda,\mu,z}\Big|_{x=x^\dagger,\gamma=0} = \begin{bmatrix} L_x \\ L_\lambda \\ L_\mu \\ L_z \end{bmatrix}\Bigg|_{x=x^\dagger,\gamma=0} = \begin{bmatrix} F_x + G_x^T \cdot \lambda + H_x^T \cdot \mu \\ G(x)^T \\ H(x)^T + z \\ \mu^T [z] - \gamma \cdot I \end{bmatrix}\Bigg|_{x=x^\dagger,\gamma=0} = 0 \tag{40}$$

Where

$x^\dagger$ is a vector of primal independent variables at the optimality point.

$[z]$ is a diagonalized matrix of vector z.

I is an identity matrix.

Therefore the optimality checking conditions $C_1 \sim C_4$ are set up as given in (41). C_1 is the stationary condition, which ensures that $x^\dagger$ is the unique optimum in a convex problem; C_2 is the feasibility condition which satisfies all equality and inequality constrains; C_3 is the complementary condition to ensure that the barrier parameter is close to zero at the optimality point; and C_4 is an additional objective condition to verify that the objective function value reaches an equilibrium point; k is the iteration number. When all four

conditions are satisfied simultaneously at a feasible solution $x^\dagger$, then the latter is considered an exclusive globally strict constrained optimality point for second-order convex problems, and is therefore applicable to most steady state optimal power flow problems.

$$
\begin{aligned}
C_1 &= L_x \to 0 \\
C_2 &= \max\{L_{\lambda_G}, L_{\lambda_H}\} \to 0 \\
C_3 &= \mu^T \cdot [z] \to 0 \\
C_4 &= F^{k+1}(x) - F^k(x) \to 0
\end{aligned}
\tag{41}
$$

F. Newton's Iterative Method to Solve for Optimality

The optimality point of KKT conditions can be solved using Newton's iterative method. Such an iterative update uses the Hessian matrix (the second order derivative) of Lagrange function as:

$$
\nabla^2 L_{x,\lambda,\mu,z} =
\begin{bmatrix}
\nabla^2 L_{xx} & \nabla^2 L_{x\lambda} & \nabla^2 L_{x\mu} & \nabla^2 L_{xz} \\
\nabla^2 L_{\lambda x} & \nabla^2 L_{\lambda\lambda} & \nabla^2 L_{\lambda\mu} & \nabla^2 L_{\lambda z} \\
\nabla^2 L_{\mu x} & \nabla^2 L_{\mu\lambda} & \nabla^2 L_{\mu\mu} & \nabla^2 L_{\mu z} \\
\nabla^2 L_{zx} & \nabla^2 L_{z\lambda} & \nabla^2 L_{z\mu} & \nabla^2 L_{zz}
\end{bmatrix}
\tag{42}
$$

$$
\nabla^2 L \cdot [\Delta x \quad \Delta\lambda \quad \Delta\mu \quad \Delta z]^T = -\nabla L
\tag{43}
$$

In general, the L_{xx} entry in the Hessian of Lagrange is obtained (45). And other entries can be found accordingly following the same procedure.

$$
\nabla^2 L_{xx} = \nabla^2 F_{xx} + \nabla^2 G_{xx}(\lambda) + \nabla^2 H_{xx}(\mu)
\tag{44}
$$

Some step size control methods [16] can be applied to improve convergence speed.

Each node and branch element is assumed with full three-phase structure. And all variables and terms are assumed representing three-phase parts. The empty phase elements will be removed before actual calculation to improve algorithm performance.

G. General Flow Chart of OPF

A flow chart of proposed OPF algorithm is shown in Fig. 4.

1. Create system model from initial configurations

2. Select algorithm solver: PBM or CIM

3.1 Determine problem dimensions

3.2 Define independence variables x and Lagrangian primal variable z and dual variables λ and μ
$$\chi = [x, \lambda, \mu, z]^T$$

4. Evaluate function values and their 1st and 2nd order derivatives for cost F and constraints G and H.

5. Check optimality conditions $C_1 \sim C_4$

6. Evaluate Hessian matrix $\nabla^2 L$

7. Calculate variable updates $\chi^{k+1} = \chi^k + \Delta\chi$

8. Repeat steps $4 - 5$.

Newton's Iterations

Fig. 4 General Flow Chart of the Three-Phase OPF Algorithm

IV. RESULTS

This section presents illustrative test results and discussions on two different IEEE distribution test feeders with various configurations and security constrains.

The first test system is the IEEE-34 test feeder – a well-known benchmark test feeder for system analysis. It has high r/x ratio conductors to serve various types of unbalanced loads in radial structure. The far end nodes with relatively large demands usually cause challenging security problems from significant low voltages. A modified system diagram with DG integration is shown in Fig. 5. A second test system – the IEEE-123 test feeder is also used. This radial system can change into possible loop structure by operating the circuit switches as shown in Fig. 6.

The nodal voltage limits are assumed between 0.925 to 1.075 pu, unless specified.

Several test cases are designed to demonstrate the performance of the proposed OPF algorithm on the two modified IEEE test feeders. DGs are added in both systems as three-phase or single-phase active sources. The location and size are determined based on the demand distribution and the distance to the substation. The generation costs at the substation are based on quadratic functions to represent the aggregated transmission or sub-transmission supply. Piecewise costs are adopted for the DGs in order to create complex combinations of different cost types as well as to be able to verify results easily in an intuitive manner. The generation cost parameters are given in TABLE IV and TABLE V for the two systems. The piecewise costs of DGs are designed with various price segments that have multiple cross points with substation supply cost in order to create a competitive scenario.
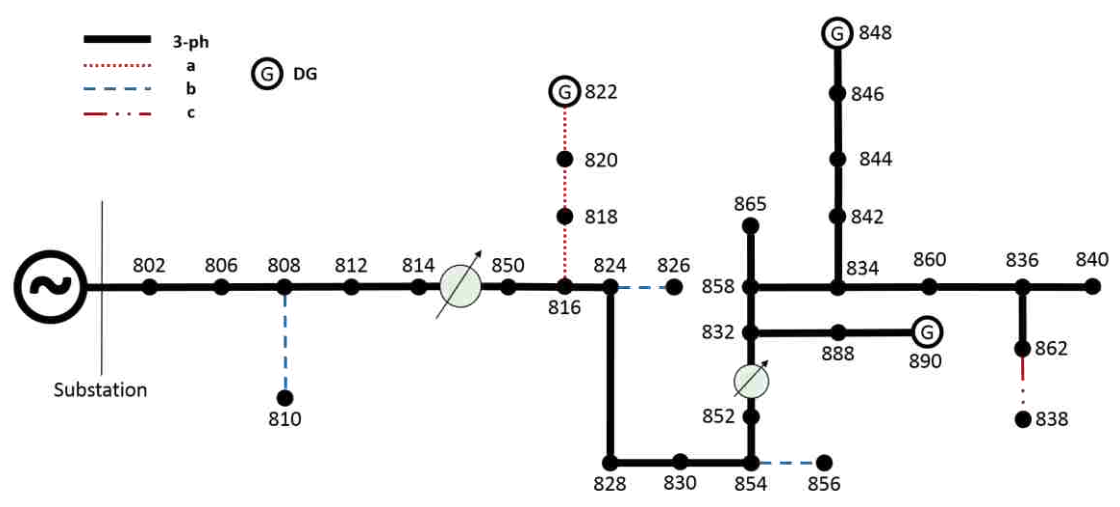
Fig. 5 Diagram of the modified IEEE-34 with DGs.
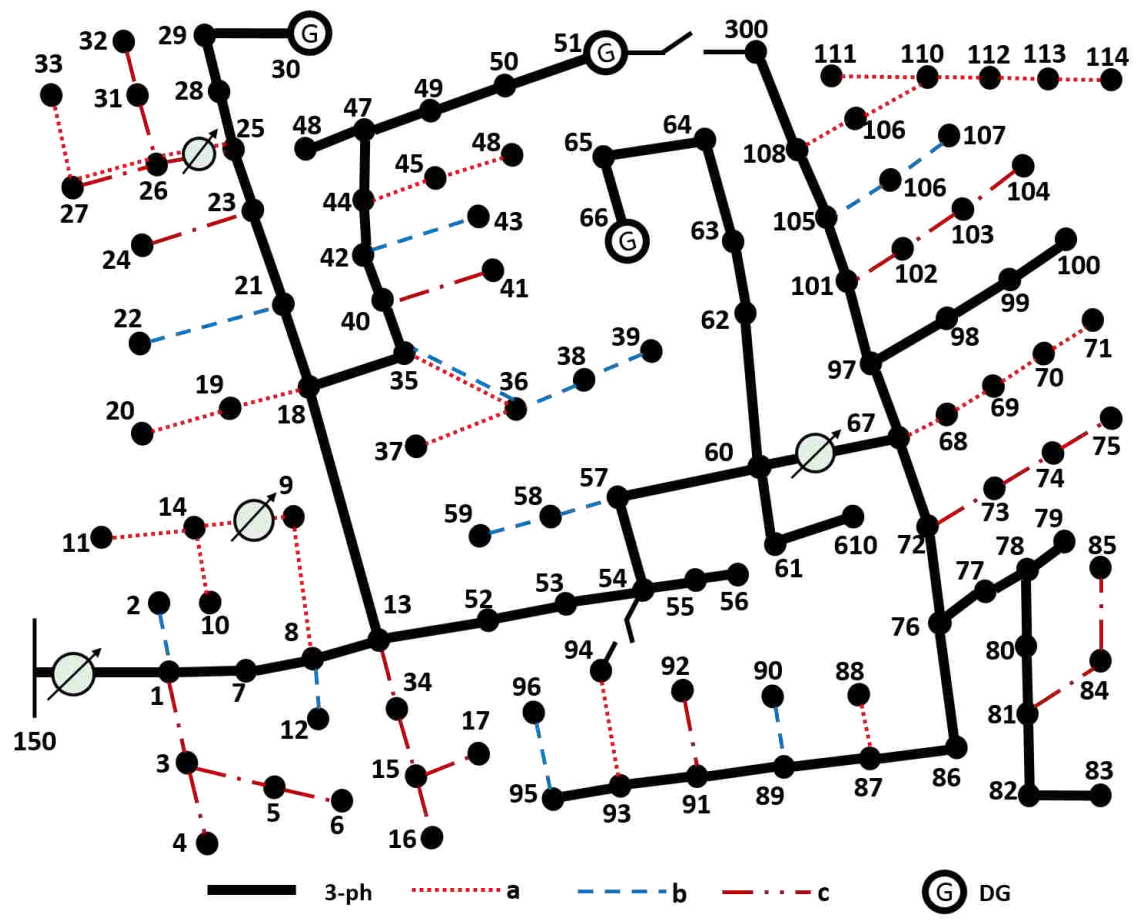
Fig. 6 Diagram of the modified IEEE-123 with DGs.

TABLE IV
GENERATION CAPACITY AND COST IN IEEE-34 TEST FEEDER

Node	Pmax (kW)	a_0		a_1		a_2	
800	1500	150		25		0.25	
		P_1 (kW)	Price$_1$ ($/MWh)	P_2 (kW)	Price$_2$ ($/MWh)	P_3 (kW)	Price$_3$ ($/MWh)
822	50	25	20	40	24	50	28
848	200	70	15	160	20	200	27
890	200	50	10	150	20	200	26

TABLE V
GENERATION CAPACITY AND COST IN IEEE-123 TEST FEEDER

Node	Pmax (kW)	a_0		a_1		a_2	
150	2000	150		25		0.25	
		P_1 (kW)	Price$_1$ ($/MWh)	P_2 (kW)	Price$_2$ ($/MWh)	P_3 (kW)	Price$_3$ ($/MWh)
66	400	136	15	288	20	400	32
51	400	200	10	320	20	400	23
30	160	50	18	112	23	160	28

Tests *1.a* and *1.b* present the OPF results using both PBM and CIM models on the IEEE-34 and 123 test feeders respectively. Test *2* is designed on looped IEEE-123 to test congestion management using OPF.

A. Test 1.a – Convergence Test on IEEE-34

Results on the IEEE-34 bus system are given in TABLE VI. DGs at nodes 822, 848 and 890 inject power at full capacity since the prices of the next segments are higher than the utility supply cost, which is determined by the optimality point. So the marginal generation costs are set by the values at the substation.

The nodal voltages, especially the minimum at the far end of the feeder (e.g. node 890), is raised significantly to 0.9702 pu compared with the original value 0.9167 pu [18]. It is noted that the active power injections contribute significantly to help regulate node voltages. This observation is true for most distribution networks whose conductors have high r/x ratios (≥ 1). The tap positions of regulators located at nodes 814 and 852 are set to zero in this test.

Results obtained from PBM and CIM are almost identical. The maximum numerical mismatch is 0.51%. The convergence in both cases is evaluated by the four optimality checking condition $C_1 \sim C_4$ as discussed earlier in Section III.C. The optimality checking conditions and the objective function value F are shown in TABLE VII and TABLE VIII respectively. For the IEEE-34 bus system, both the CIM and PBM show fast convergence within 14 and 20 iterations, respectively. The computation times shown in the Table VII and Table VIII are measured as the average elapsed time for 20 repeated complete runs.

TABLE VI
RESULTS IN TEST 1.*a* USING CIM AND PBM

Node	CIM			PBM		
	Pg-A (kW)	Pg-B (kW)	Pg-C (kW)	Pg-A (kW)	Pg-B (kW)	Pg-C (kW)
800	315.785	289.494	238.510	317.251	292.024	239.950
822	40.000	n/a	n/a	40.000	n/a	n/a
848	160.000	160.000	160.000	160.000	160.000	160.000
890	150.000	150.000	150.000	149.998	150.000	150.000
Vmax(pu)	1.0500	1.0500	1.0500	1.0500	1.0500	1.0500
Vmin(pu)	0.9758	0.9702	0.9781	0.9711	0.9668	0.9753
Marginal Gen Cost ($/h)	25.16 at 800-A	25.15 at 800-B	25.12 at 800-C	25.16 at 800-A	25.15 at 800-B	25.12 at 800-C

TABLE VII
CONVERGENCE PERFORMANCE IN TEST 1.*A* USING CIM

Ite	C_1	C_2	C_3	C_4	F
1	0.008115	112.4526	44.00779	0.140844	439.12
2	3.11E-04	13.68686	8.110502	0.356865	487.79
3	1.45E-05	2.185336	2.151183	5.38E-02	488.81
⋮					
13	8.47E-10	6.55E-09	7.25E-08	2.02E-05	487.99
14	6.20E-11	5.04E-10	7.25E-09	9.73E-08	487.99
Computation time (s)			1.063		

TABLE VIII
CONVERGENCE PERFORMANCE IN TEST 1.*A* USING PBM

Ite	C_1	C_2	C_3	C_4	F
1	0.004004	154.876	30.72852	0.006466	441.12
2	0.001039	28.15607	11.86665	0.003224	488.03
3	0.000626	26.95201	14.32705	0.002562	488.94
⋮					
19	3.25E-07	6.12E-05	4.76E-11	1.54E-05	488.00
20	1.21E-07	3.70E-05	4.90E-12	1.52E-05	488.00
Computation time (s)			0.688		

B. Test 1.b – Convergence Test on IEEE-123

On the larger IEEE-123 bus test system, the results of PBM/CIM are identical with a maximum mismatch of 0.002% in voltage and generation outputs, as shown in TABLE IX. The DG at node 51 is injecting at full capacity while the DGs at node 66 and 30 are dispatched at lower power due to higher prices. The marginal generation is the utility supplier at the substation. The voltages are within security limits with zero taps changing at voltage regulators at nodes 9, 25 and 60.

On the larger system, the CIM takes longer time to converge mainly due to the increasing dimensions of matrix and vectors in the computation process, which may be significantly improved by sparse matrix techniques as shown in [17]. But the number of iterations to convergence (see TABLE X) is just slightly increased in the CIM, while the PBM starts showing relatively slower converging trajectory (especially on the feasibility condition C_1) and larger number of iterations needed to converge (see TABLE XI). This is mainly caused by the complex number matrix calculation in the Newton's iterative loop.

Based on the results of tests *1.a* and *1.b*, both the CIM- and PBM-based OPF show good and accurate performance in solving typical distribution networks. However, the CIM is a preferred method to solve large and complex system for a more robust performance, while the PBM can be used to solve relatively smaller systems for faster computation speeds.

TABLE IX
RESULTS IN TEST 1.b USING CIM AND PBM

Node	CIM			PBM		
	Pg-A (kW)	Pg-B (kW)	Pg-C (kW)	Pg-A (kW)	Pg-B (kW)	Pg-C (kW)
150	639.882	176.859	377.770	639.869	176.860	377.763
66	288.000	288.000	288.000	288.000	288.000	288.000
51	400.000	400.000	400.000	400.000	399.999	399.999
30	112.000	112.000	112.000	112.000	112.000	112.000
Vmax(pu)	1.0438	1.0462	1.0438	1.0438	1.0462	1.0438
Vmin(pu)	0.9782	1.0142	1.0088	0.9782	1.0142	1.0088
Marginal Gen Cost ($/h)	25.32 at 150-A	25.09 at 150-B	25.19 at 150-C	25.32 at 150-A	25.09 at 150-B	25.19 at 150-C

TABLE X
CONVERGENCE PERFORMANCE IN TEST 1.b USING CIM

Ite	C_1	C_2	C_3	C_4	F
1	51.7955	0.0033	1692.8266	0.1360	520.38
2	3.3166	0.0027	871.9468	0.0734	524.80
3	0.4824	0.0010	221.0387	0.2213	530.01
:					
18	1.09E-10	1.92E-11	8.12E-09	5.91E-06	521.34
19	1.34E-11	2.47E-12	8.12E-10	5.82E-07	521.34
Computation time (s)			10.259		

TABLE XI
CONVERGENCE PERFORMANCE IN TEST 1.b USING PBM

Ite	C_1	C_2	C_3	C_4	F
1	44.0212	0.0015	1390.0520	0.2165	520.82
2	2.0822	0.0013	689.1914	0.0168	523.20
3	0.3376	0.0002	174.4113	0.2106	529.84
:					
30	2.44E-05	1.23E-08	4.80E-17	1.40E-08	521.35
31	3.37E-08	1.02E-08	2.44E-17	2.75E-08	521.35
Computation time (s)			5.805		

C. Test 2 – Over Loading Management Test on Looped IEEE-123

Distribution systems are usually designed with overrated loading limits on feeders and laterals to guarantee system security; congestion is rarely studied in distribution system. However, many modern distribution networks have adopted loop or even meshed structures in U.S., Europe and Asian countries. For the next set of tests, the IEEE-123 bus system is modified to create a congestion contingency in order to test the ability of OPF algorithm to solve more complex system under imposed voltage and line loading constraints. Stricter voltage limits of 0.95 to 1.05 pu is applied and the original voltage regulator taps [18] are used merely for testing of the algorithm.

A loop structure is created in the middle part of the feeder system by closing the switch 51-300. Initially, results are obtained on such a loop system without the enforced line flow limits, as shown on the left columns in TABLE XII. Voltages are shown at DG nodes and at the voltage regulator after the substation. The DG at node 66-B injects slightly less power than in test *1.b* due to the fact that the nodal voltage is already at the upper limit of 1.05 pu. It is noted that most branches within the loop area have lower branch flows compared to the radial case.

By observation of branch flows in TABLE XIII, branch 60-67 has relatively higher line flow (425.54 kVA on phase-A), so a loading limit of 400 kVA is enforced on this branch to create a congestion contingency. We run the OPF algorithm again and the generations at node 66 phases A and B are reduced to relieve the overloading problem. The substation injects more power (more expensive power) to balance the mismatch and therefore increases the system marginal generation cost. The branch flow along 60-67 shows that it is constrained to the limited value. The results show system loss increase at

the congested phase just as expected. However, the uncongested phases show losses behave according to system structure and conductor mutual coupling.

The nodal shadow prices for active power (the Lagrange dual variable λ_P) at nodes 67 increased from 25.03 ($/h) and 47.12 ($/h) while that at node 60 decreased from 25.01 ($/h) to 14.34 ($/h) which indicate the cost to re-dispatch generation to relieve the congestion. Such pricing signals may be used by the DNO to do extended economic analysis.

TABLE XII
GENERATION (IN KW) AND VOLTAGE (IN PU) RESULTS IN TEST 2

Node	Non-Congested			Congested		
	Pg-a	Pg-b	Pg-c	Pg-a	Pg-b	Pg-c
150	648.136	177.693	382.110	720.557	237.152	383.457
66	288.000	282.508	288.000	164.257	221.258	288.000
51	400.000	400.000	400.000	400.000	400.000	400.000
30	112.000	112.000	112.000	112.000	112.000	112.000
Node	V-a	V-b	V-c	V-a	V-b	V-c
149	1.0438	1.0438	1.0438	1.0438	1.0438	1.0438
66	1.0145	1.0500	1.0202	0.9999	1.0500	1.0223
51	1.0244	1.0396	1.0331	1.0209	1.0405	1.0337
30	1.0172	1.0446	1.0258	1.0163	1.0435	1.0274
Vmax	1.0450	1.0500	1.0444	1.0438	1.0500	1.0448
Vmin	1.0013	1.0296	1.0161	0.9959	1.0313	1.0164
MGC($/h)	25.34	25.09	25.19	25.36	25.12	25.19
Ploss %	1.447	0.918	1.185	1.490	0.691	1.255

TABLE XIII
BRANCH FLOW (KVA) RESULTS ON SELECTED LINES IN TEST 2

From	To	Non-Congested			Congested		
		Sf-a	Sf-b	Sf-c	Sf-a	Sf-b	Sf-c
13	18	206.648	142.569	39.011	188.760	145.007	39.236
13	52	473.048	188.537	296.668	531.024	217.521	297.862
18	35	115.892	160.129	38.847	142.027	166.493	39.550
60	67	425.536	204.118	326.297	399.999	195.500	326.953
67	72	294.69	314.358	331.734	292.898	314.743	331.829
67	97	307.144	181.63	232.354	308.636	188.763	232.412
51	300	299.609	247.195	228.156	319.469	256.594	227.736
λ_P at 60 ($/h)		25.01	23.56	24.25	14.34	23.45	23.44
λ_P at 67 ($/h)		25.03	23.59	24.33	47.12	23.45	23.77

V. CONCLUSION

A future distribution network is envisioned with massive DG integration and digitalized communication platform. An unbalanced three-phase OPF algorithm using PDIPM is proposed and tested for providing constrained dispatch to minimize the total generation costs from transmission and DG suppliers. The program considers comprehensive details of components and devices and is general enough to solve radial or meshed distribution systems. The program can be used as a primary analysis tool for the DNO to solve optimal operation of DGs with different types of energy cost functions while satisfying the voltage and line loading security constraints. The algorithm shows fast convergence on IEEE test feeders with various system configurations and constraints. The test results also show the potential value of the OPF algorithm for the DNO to perform extended studies on congestion management, system planning, impact of conservative voltage reduction contingency analysis, and the effects of regulatory policies.

REFERENCES

[1]   N. Hadjsa id and J. Sabonnadi ère, *Power Systems and Restructuring*. London, Wiley, 2009.

[2]   H. Willis, R. Schrieber, and G. Welch, *Aging Power Delivery Infrastructures*. Dekker, 2007.

[3]   Office of Electric Transmission and Distribution, U.S. Dept. of Energy, "Grid 2030: A National Vision for Electricity's Second 100 Years," Jul 2007 [online]. Available: http://energy.gov/

[4]   U.S. Department of Energy, "2010 Smart Grid System Report," Feb 2012 [online]. Available: https://www.smartgrid.gov/

[5]   U.S. D.O.E, "The Potential Benefits Of Distributed Generation And Rate-Related Issues That May Impede Their Expansion," Feb 2007.

[6]   Energy Regulatory Commission (CRE) in France. Available online: http://www.cre.fr/en

[7]   J. Kumagai, "The Rise of the Personal Power Plant," *IEEE Spectrum,* May 2014 [online]. Available: http://spectrum.ieee.org/

[8]   F. Beck and E. Martinot, "Renewable energy policies and barriers," in Encyclopedia of Energy. London, U.K.: Academic/Elsevier Science, 2004, pp. 365–383.

[9]   R. G. Wasley and M. A. Shlash, "Newton-Raphson Algorithm for 3-phase Load Flow," *Proceedings of the Institution of Electrical Engineers*, vol. 121, no. 7, pp. 630 – 638, 1974.

[10]   P. Garcia, J. Pereira, S. Carneiro, Jr., V. Costa and N. Martins, "Three-Phase Power Flow Calculations Using the Current Injection Method," *IEEE Transactions on Power System*, vol. 15, no. 2, May 2000.

[11]   W. H. Kersting, "Distribution System Modeling and Analysis," CRC Press, New York, NY, 2007.

[12]   A. Forsgren, P.E. Gill, and M.H. Wright, "Interior Method for Nonlinear Optimization," *Review of Society for Industrial and Applied Mathematics*, vol. 44, No. 4, pp. 525-597, Aug. 2006.

[13]   L. R. Araujo, D. R. R. Penido, S. Carneiro, Jr., and J. L. R. Pereira, "A Three-Phase Optimal Power-Flow Algorithm to Mitigate Voltage Unbalance," *IEEE Transactions on Power Delivery*, vol. 28, no. 4, Oct 2013.

[14]   Y. Cao, Y. Tan, C. Li, and C. Rehtanz, "Chance-Constrained Optimization-Based Unbalanced Optimal Power Flow for Radial Distribution Networks," *IEEE Transactions on Power Delivery,* vol. 28, no. 3, Jul 2013.

[15]   G. T. Heydt, B. H. Chowdhury, M. L. Crow, D. Haughton, B. D. Kiefer, F. Meng and B. R. Sathyanarayana, "Pricing and Control in the Next Generation Power Distributed System," *IEEE Trans. on Smart Grid*, Vol. 3, No. 2, pp. 907-914, Jun 2012.

[16]   R. D. Zimmerman, C. E. Murillo- Sánchez, and R.J. Thomas, "MATPOWER: Steady-State Operations, Planning and Analysis Tools for Power Systems Research and Education," *IEEE Trans. on Power Systems,* vol. 26, no. 1, p. 12-19, Feb. 2011.

[17] M. Crow, *Computational Methods for Electric Power Systems.* 2nd ed. CRC, 2009.

[18] IEEE PES Distribution System Analysis Subcommittee's Distribution Test Feeder Working Group [online]. Available: http://www.ewh.ieee.org/soc/pes/dsacom/testfeeders/index.html

[19] M. Chen, and T. Chen, "Application of Three-Phase Load Flow to Power System Distribution Automation," *IEE International Conference on Advances in Power System Control, Operation and Management,* Nov 1991.

[20] U.S. Energy Information Administration, "Annual Energy Outlook 2012." Available online: http://www.eia.gov/forecasts/aeo.

[21] Power System Engineering Research Center, "Implications of the Smart Grid Initiative on Distribution Engineering." Available online: http://www.pserc.wisc.edu/research/public_reports.aspx

[22] R. Byrd, J. Nocedal, R. Waltz, and Y. Wu, "On the Use of Piecewise Linear Models in Nonlinear Programming," *Mathematical Programming,* vol. 137, no. 1-2, pp. 289 – 324, Feb 2013.

[23] V. Costa, N. Martins, and J. Pereira, "Development in the Newton Raphson Power Flow Formulation Based on Current Injections," *IEEE Transactions on Power Systems,* vol. 14, no. 4, Nov 1999.

[24] D. Penido, L. Araujo, S. Carneiro, Jr., J. Pereira, and P. Garcia, "Three-Phase Power Flow Based on Four-Conductor Current Injection Method for Unbalanced Distribution Networks," *IEEE Transactions on Power Systems,* vol. 23, no. 2, May 2008.

[25] Y. Yao, J. Shan, D. Wang, and L. Liu, "An Improved Newton Power Flow in Rectangular Form for Systems with Small Impedance Branches", *2nd International Conference on Power Electronics and Intelligent Transportation System (PEITS),* 2009.

III. Optimal Operation and Control with Distributed Energy Resources and Solid State Transformers in Future Distribution Systems

F. Meng, Student Member, *IEEE*,   D. Shah, Student Member, *IEEE*,

B. Chowdhury, Senior Member, *IEEE*,   M. L. Crow, Fellow, *IEEE*

Abstract — **Power distribution systems are evolving toward a smart grid paradigm facilitated by infrastructure improvement, innovative technologies, and power electronic interface devices. A three-phase unbalanced OPF algorithm using primal-dual interior point method (PDIPM) is proposed for the next generation of distribution networks featuring massive distributed energy resources (DER) and solid state transformers (SST). The algorithm is developed as a generalized program that can be customized to incorporate new component models or system constraints. The topology and functionalities of the SST are introduced and modeled in the OPF algorithm. Comprehensive models of loads, conductors, voltage regulators and transformers are modeled for accuracy of analysis. Simulation tests on IEEE test feeders show that the OPF algorithm can be used as part of a distribution automation enterprise to optimize operations of distributed generation and storage in conjunction with the SST to improve system economic efficiency, DER penetration, and voltage profiles.**

Index Terms — **Unbalanced optimal power flow; primal-dual interior point method; solid state transformer.**

I. INTRODUCTION

The electric power industry is undergoing profound changes as it moves toward a smart grid (SG) paradigm to achieve higher levels of energy efficiency, renewable energy source integration, economic benefits, and system reliability and security [1]. Most restructuring thus far has taken place at the transmission or sub-transmission levels, while most distribution systems continue to operate as monopolies with aging infrastructures. Traditional distribution providers have limited generation purchase options; they generally procure power at wholesale prices from generation companies in the forward and/or futures market, and sometimes in the spot market, and supply their customers directly through distribution feeders at fixed electricity rates set by regulatory bodies [2].

The distribution systems of today are beginning to feel the urgency to adopt a vastly different operational paradigm wherein an entity like a distribution network operator (DNO) can take a more active role in command and control under the advocacy of increasing DER penetrations and better financial benefits and quality of energy service to customers [3]. Several examples of real system operation have already presented preliminary successful experiences to build the next generation of distribution network with competitive environment and open access energy markets for DERs [4].

DERs are small sized power generation units located at or close to customers. Various types of DERs are currently available. These include conventional or micro-turbine generators (fueled by natural gas, diesel fuel, etc.) and renewables (wind, solar photovoltaic or solar thermal, biomass, etc). In the envisioned open distribution network, the DER owners will be allowed to participate in economic operations as independent entities or market players [2], [5] and [6]. The generation costs may either be evaluated

using quadratic functions (e.g. for fuel consuming types) or using piecewise linear bidding segments, which will be discussed in details in Section II.B. The technologies of energy storage and advanced power electronics also enhance system performance by mitigating the intermittent nature of some types of renewable generations [3].

The solid state transformer (SST) is an advanced electronic device for future distribution systems [7]. Besides the reduced size and weight compared to the conventional iron-core type transformers, it provides several novel features such as: customer side voltage regulation; plug-and-play capability for DERs, electric vehicles, energy storage or any other types of resources; reactive power support at the primary feeder side; digital measurement and communication. Each SST can either work in unity power factor (UPF) control mode as default, or in active var control mode. The later enables the SST to operate as a controllable reactive power source that can be optimally controlled by the DNO using OPF analysis.

Recent advancements in the power semiconductor technology has accelerated the utilization and commercialization of the SST, which has raised its potential to replace or supplement the conventional distributed transformers [8] − [11]. An empirical design criterion for distribution SSTs is proposed in [12] to address the frequency domain stability analysis and solve the harmonic resonance [13]. Recent research efforts are targeting a MVA substation level SST [14]-[15].

The increasing DER penetration and implementation of solid state controllers can create new challenges associated with bi-directional power flows in distribution networks. This new phenomenon necessitates new smart grid control schemes which are essentially lacking in the current operating paradigm. The purpose of these schemes is to

optimally aggregate the energy mix by combining the profitability of each resource while satisfying system security constraints.

In this paper, a three-phase unbalanced OPF algorithm is proposed to solve for optimal operation of DERs and SSTs using the primal-dual interior point method (PDIPM) [16]. The algorithm is adaptive to handle comprehensive models of constant impedance, current, or power (*ZIP*) loads and different branch elements. It may be customized to adopt new devices or new constraints. The modifications to OPF formulation from SST implementation is categorized and included in the OPF algorithm. The algorithm adopts a rectangular coordinate format as used in current injection method (CIM) power flow analysis [17] to improve the performance.

The proposed OPF algorithm has the following features:

- Capability to solve for optimality point of DER and SST operations under different system configurations.

- Adaptability to incorporate new customized devices or constraints by modifying the variables, constraints and even objective functions.

- Ability to include demand response and energy storage for more comprehensive analysis.

- Potential for use in short or long term optimal planning by simply substituting the objective function with planning cost minimization.

Next we describe the models for each element in the distribution network.

II. DISTRIBUTION NETWORK MODELING

A. Conductor, Transformer and Voltage Regulator

A pi-model for branch elements in distribution network is shown in Fig. 1. The general equations relating the nodal voltages at both ends of the branch (V_i and V_j) and the branch currents at the two ends (I_i and I_j) are given in (1) and (2).

$$\begin{bmatrix} I_i^{abc} \\ I_j^{abc} \end{bmatrix} = \begin{bmatrix} Y_{ii} & Y_{ij} \\ Y_{ji} & Y_{jj} \end{bmatrix} \begin{bmatrix} V_i^{abc} \\ V_j^{abc} \end{bmatrix} \tag{1}$$

$$Y_{ii} = C_{ii} \cdot \frac{Y_A}{a_T a_T^*} + Y_B \qquad Y_{ij} = C_{ij} \cdot \frac{Y_A}{a_T^*}$$

$$Y_{ji} = C_{ji} \cdot \frac{Y_A}{a_T} \qquad Y_{jj} = C_{jj} \cdot Y_A + Y_B \tag{2}$$

where

Y_A and Y_B are the three-phase series and shunt admittance matrix of branch element, respectively.

a_T is the three-phase voltage ratio matrix considering angle shift.

C_{kk}, $k = \{i, j\}$, are the transform matrices that are defined in TABLE I.
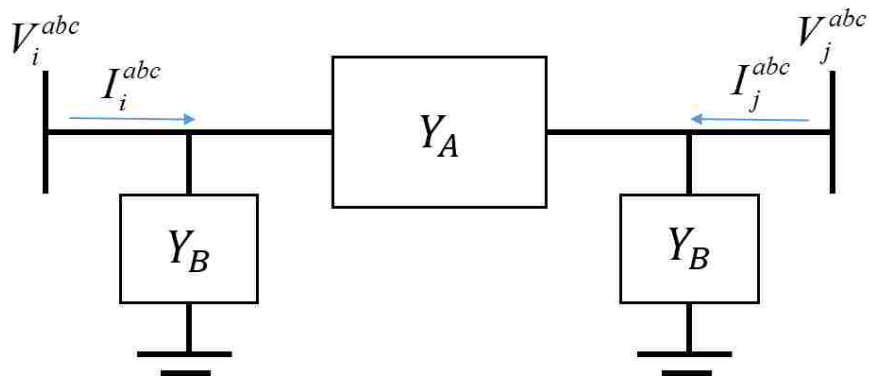
Fig. 1 π-model diagram for branch elements.

TABLE I
TRANSFORM MATRICES OF SELF AND MUTUAL ADMITTANCE FOR BRANCH ELEMENTS

Branch Element		Self Admittance		Mutual Admittance	
		C_{ii}	C_{jj}	C_{ij}	C_{ji}
Conductor		C_I	C_I	C_I	C_I
Transformer or voltage regulator	Y-G -- Y-G	C_I	C_I	C_I	C_I
	Delta -- Delta	C_{II}	C_I	C_{III}	C_{III}
	Delta -- Y-G	C_{II}	C_{II}	C_{II}	C_{II}

$$C_I = \begin{bmatrix} 1 & 0 & 0 \\ 0 & 1 & 0 \\ 0 & 0 & 1 \end{bmatrix}, C_{II} = \frac{1}{3} \cdot \begin{bmatrix} 2 & -1 & -1 \\ -1 & 2 & -1 \\ -1 & -1 & 2 \end{bmatrix}, C_{III} = \frac{1}{\sqrt{3}} \cdot \begin{bmatrix} -1 & 1 & 0 \\ 0 & -1 & 1 \\ 1 & 0 & -1 \end{bmatrix}$$

The detailed models of each type of conductor will be explained in the following parts.

1) Conductor

The impedance matrix of the untransposed 3-wire or 4-wire conductors can be calculated using Carson's equations [20]. The series admittance matrix Y_A is the phase admittance matrix of the conductor, and the shunt matrix Y_B is the susceptance matrix. Since all conductor segments are connected in wye or wye-ground with no off-normal tap ratio changing, the voltage ratio matrix a_T and the transform matrices C_{kk} are all diagonal identity matrix (C_I).

2) Transformer

Three-phase transformers in distribution systems may have many different connections (wye, wye-G, and delta) at the primary and secondary sides. The voltage ratio matrix a_T are usually specified in system configuration. The transform matrices C_{kk} are listed in Table for three most commonly used connection types.

3) Voltage regulator

Voltage regulators are important devices in conventional distribution network to regulate or compensate voltage drops along the feeder. They can be treated as special autotransformers with a load tap changing mechanism. Standard step regulators contain a reversing switch enabling a ± 10% regulating range of voltages, usually in 32 steps. Assuming the tap changing is installed at the primary side, the equivalent voltage ratio matrix a_T is basically determined by the tap positions and the types of regulator (type A or type B) [20].

$$a_T = 1 \pm 0.00625 \cdot Tap^{abc} \tag{3}$$

Where

$Tap^{abc} = \pm\ 1, 2, \ldots, 16.$

$-$ sign for Type B/A at raise/lower positions

$+$ sign for Type B/A at lower/raise positions

After obtaining all branch element admittance matrices, the system nodal admittance matrix Y_{BUS} can be built in rectangular coordinate:

$$\begin{bmatrix} I_{M,1}^{abc} \\ I_{R,1}^{abc} \\ \vdots \\ I_{M,n}^{abc} \\ I_{R,n}^{abc} \end{bmatrix} = \underbrace{\begin{bmatrix} B_{11}^{abc} & G_{11}^{abc} & \cdots & B_{1n}^{abc} & G_{1n}^{abc} \\ G_{11}^{abc} & -B_{11}^{abc} & & G_{1n}^{abc} & -B_{1n}^{abc} \\ \vdots & & \ddots & & \vdots \\ B_{n1}^{abc} & G_{n1}^{abc} & & B_{nn}^{abc} & G_{nn}^{abc} \\ G_{n1}^{abc} & -B_{n1}^{abc} & \cdots & G_{nn}^{abc} & -B_{nn}^{abc} \end{bmatrix}}_{Y_{BUS}} \cdot \begin{bmatrix} V_{R,1}^{abc} \\ V_{M,1}^{abc} \\ \vdots \\ V_{R,n}^{abc} \\ V_{M,n}^{abc} \end{bmatrix} \tag{4}$$

Where

I_R, I_M, V_R, and V_M are the real and imaginary parts of complex current and voltage, respectively.

G_{BUS}^{abc} and B_{BUS}^{abc} are the three-phase conductance and susceptance matrices in nodal matrix Y_{BUS}.

By ordering the rows and columns, Y_{BUS} can be rewritten in decoupled format of real and imaginary parts as:

$$\begin{bmatrix} I_R^{abc} \\ I_M^{abc} \end{bmatrix} = \begin{bmatrix} Y_{RR} & Y_{RM} \\ Y_{MR} & Y_{MM} \end{bmatrix} \begin{bmatrix} V_R^{abc} \\ V_M^{abc} \end{bmatrix} \tag{5}$$

Where

$Y_{RR} = Y_{MM} = G_{BUS}$, and $Y_{RM} = - Y_{MR} = - B_{BUS}$.

The branch admittance matrices Y^f and Y^t at *from* and *to* ends can be found, also in rectangular format, using the nodal admittance matrices and the incidence matrices C^f and C^t that indicate the node-branch connection relationship.

$$\begin{bmatrix} I_R^{f\,abc} \\ I_M^{f\,abc} \end{bmatrix} = \begin{bmatrix} Y_{RR}^f & Y_{RM}^f \\ Y_{MR}^f & Y_{MM}^f \end{bmatrix} \begin{bmatrix} V_R^{abc} \\ V_M^{abc} \end{bmatrix} \tag{6}$$

$$\begin{aligned} Y_{RR}^f = C^f \cdot Y_{RR} && Y_{RM}^f = C^f \cdot Y_{RM} \\ Y_{MR}^f = C^f \cdot Y_{MR} && Y_{MM}^f = C^f \cdot Y_{MM} \end{aligned} \tag{7}$$

The *to* end entries can be found using exactly the same formulas above by substituting *f* with *t*.

B. Nodal Injection Elements

1) ZIP load

The loads in distribution system can be categorized by the method of connection to the primary feeder as distributed or spot load, in wye or delta connection. In this study, distributed loads are converted to spot loads by lumping at the two ends of the line segment with proportion factors *a* and *1-a* ($0 \le a \le 1$) respectively. The loads can also be characterized as constant impedance, current or power (also known as *ZIP* loads). The equivalent power demand of *ZIP* loads S^{ZIP} is related to nodal voltage magnitudes with the relationship as:

$$S^{ZIP} = S^Z \cdot |V|^2 + S^I \cdot |V| + S^{PQ} \tag{8}$$

Such nonlinear characteristic of *ZIP* loads are included in the OPF algorithm during evaluation of the non-linear nodal balance constraints and their derivatives in order to obtain accurate calculations.

Shunt capacitor banks are commonly used to provide reactive power support and can be modeled as a special constant load given in kVar.

2) DER

DERs are controllable power injection units in the OPF algorithm. DER technologies whose primary outputs are direct current (e.g. photovoltaic and fuel cell) only inject active power. This is also applicable for those DERs whose primary outputs are alternating current (e.g. wind and microturbine) by forcing them to operate at unity power factor so as to maximize the energy conversion efficiency.

In economic operation analysis, the DER generation costs are given either as traditional quadratic function or as piecewise price segment. The piecewise cost functions are usually expressed using pairs of constant energy cost (*$/MWh*) within specific range of generation power (*MW* or *kW*). These discontinuous segments can be converted into a continuous linear cost function f_{pw} as shown in Fig. 2 [18].

$$f_{pw}(x) = \text{price}_i \cdot (P_g - P_i) + C_{pw_i}, \quad P_{i-1} \leq P_g \leq P_i \tag{9}$$

where
   $i = 1, 2, \ldots, m$ - are sequence of price segments.

   C_{pw_i} is the cumulative cost for each segment.

The application of piecewise linear functions and the derivatives will be discussed in the next section.
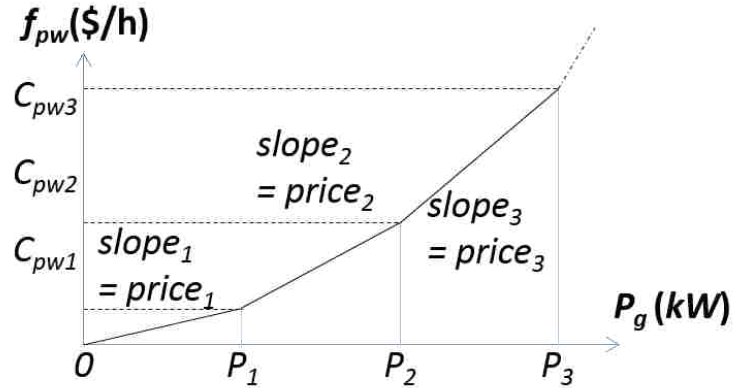
Fig. 2 Constrained piecewise cost function f_{pw}.

C. Solid State Transformer

The SST is an advanced power electronic transformer which contains three stages of single phase converters that are connected in cascaded mode: AC/DC active rectifier, dual active bridge (DAB) DC/DC converter, and DC/AC inverter, as shown in Fig. 3 in Section III. There are two DC links in SST – low voltage DC (LVDC) and high voltage DC (HVDC) – which act as buffer between the primary feeder and the load. Voltages at HVDC and LVDC are regulated to constant values by the active rectifier and DAB converter respectively. The SST node can be considered as a PQ node for power flow analysis. The net power flow at the primary side of the SST is the aggregated power injection/consumption from load and DER. In general, the SST provides several advanced features that include:

- Var injection control at the rectifier

The reactive power injection at the rectifier primary side is regulated by the Q axis current I_q using a DQ vector controller [6]. The value of I_q depends on the external reactive power control signal (Q_{SST}^* in Fig. 3). SSTs in var control mode are considered

as controllable sources that can be optimally controlled by the DNO using the OPF program. SSTs can also work at unity power factor (UPF) mode without external Var control signals.

- Plug-and-play hub for DERs and other resources

    The LVDC serves as plug-and-play coupling hub, with constant regulated voltage, for DER or other types of distributed resources in either AC or DC types.

- Voltage regulation at load side

    The third stage inverter provides 1.0 pu AC voltage output to loads under normal conditions and also during voltage sag/swell events [7]. This exclusive functionality significantly improves the power quality and reliability in energy services. Also, the constant terminal voltage will equivalently change the *ZIP* load intro constant *PQ* load.

- Reactive power filtering

    The reactive power demand and injection from load and DER are filtered out at DAB and the DC links, as long as there is enough kVA rating at the converter. As a result, the reactive power at the primary side of the SST is only determined by SST var control in both UPF and var control modes, while the gateway active power is the net injection/consumption from DERs and loads. Recent research shows that the capacity rating of all three stages in the SST has increased to 270 kVA or at similar level. And multiple SSTs can be connected in parallel to serve a large number of aggregated customers at the same node [21]. It is important for the DNO and customer to size the load and DER according to the SST ratings during system design or restructuring.

$$S_{REC} = S_{DAB} = S_{REC} = S_{SST} \tag{10}$$

$$|S_{load}| \leq S_{SST} \tag{11}$$

$$|S_{DER} - S_{load}| \leq S_{SST} \tag{12}$$

The above features and constraints of the SST implementation will be discussed and modeled in Section III.C.

III. THREE-PHASE UNBALANCED OPF ALGORITHM

A. *Generalized OPF Using PDIPM.*

The general OPF formulation is given in rectangular coordinate format in Eqs. (13) – (18). The objective function F is to minimize the sum of generation costs f.

$$\text{Min: } F(x) = \sum(f(x)) \tag{13}$$

s.t.

$$x = [x_1 \ x_2 \ x_3 \ x_4 \ x_5]^T = [V_R \ V_M \ P_g \ Q_g \ x_Z]^T \tag{14}$$

$$f(\mathrm{x}) = [f_{poly}(x), f_z(x)]^T \tag{15}$$

$$G(x) = 0 \tag{16}$$

$$H(x) \leq 0 \tag{17}$$

$$X_{min} \leq x \leq X_{max} \tag{18}$$

Where

x is a vector of independent variables including:

V_R and V_M : real and imaginary parts of nodal voltage.

P_g and Q_g : active and reactive power injections from controllable DERs and other devices.

x_Z : user-defined variable

$f_{poly}(x)$ is classic quadratic generation cost.

$f_z(x)$ is user-defined cost function (e.g. piecewise).

$G(x)$ and $H(x)$ are equality and inequality system constraints.

X_{max} and X_{min} are linear upper and lower limits to variable x.

1) General formula of cost function f

The 1st and 2nd order partial derivatives of cost function f are given as

$$\nabla f(x) = f_x = \left[\begin{array}{cc} \dfrac{\partial f_{poly}}{\partial x} & \dfrac{\partial f_z}{\partial x} \end{array} \right]^T \tag{19}$$

$$\nabla^2 f(x) = \dfrac{\partial f_x^T}{\partial x} = \dfrac{\partial^2 f_{poly}}{\partial x^2} + \dfrac{\partial^2 f_z}{\partial x^2} \tag{20}$$

For quadratic cost

$$f_{poly}(x) = a_0 + a_1 \cdot Pg + a_2 \cdot Pg^2 \tag{21}$$

$$\nabla f_{poly}(x) = a_1 + 2a_2 \cdot Pg \tag{22}$$

$$\nabla^2 f_{poly}(x) = 2a_2 \tag{23}$$

The formula of piecewise cost as a customized function is discussed in part B of this section.

2) General formula of equality constraints $G(x)$

The elements in equality constraint vector $G(x)$ are explained below. λ are dual variables as Lagrange multipliers.

$$G(x) = \begin{bmatrix} G^P \\ G^Q \\ G^V \\ G^Z \\ \dots \\ G^X \end{bmatrix} \leftrightarrow \begin{matrix} \lambda^P \\ \lambda^Q \\ \lambda^V \\ \lambda^Z \\ \dots \\ \lambda^X \end{matrix} \tag{24}$$

G^P and G^Q are nonlinear nodal active and reactive power balance constraints given as the mismatch between total branch injecting power (P^{INJ} and Q^{INJ}) and nodal specified power ($P_G - P_D$) and ($Q_G - Q_D$). The corresponding dual variables λ^P and λ^Q can be used to represent the nodal shadow prices of power supply, which may be used to derive economic operation control signals [19].

$$G^P = P_{INJ} - (P_G - P_D) \tag{25}$$

$$G^Q = Q_{INJ} - (Q_G - Q_D) \tag{26}$$

Where

$$P_{INJ} = V_R \cdot I_R + V_M \cdot I_M \tag{27}$$

$$Q_{INJ} = V_M \cdot I_R - V_R \cdot I_M \tag{28}$$

I_R and I_M can be found using decoupled rectangular admittance matrices in (5)

P_G and Q_G are nodal power generation as in variables x_3 and x_4. The Var injection at SST (Q_{SST}) is also considered as a reactive power source.

P_D and Q_D are equivalent demand from *ZIP* load in (8).

The nodal voltage magnitude limit can be dealt with as nonlinear constraints in the rectangular coordinates. The equality voltage limits only apply for PV nodes (if there are any), which have the same upper and lower limits $V_{max} = V_{min}$.

$$G^V = V_R^2 + V_M^2 - V_{max}^2 \tag{29}$$

G^Z is the optional customized nonlinear equality constraint defined by the user as needed. Any variables, including customized variable x_z, with the same upper and lower limits are included in linear equality constraint G^X. A_{EQ} is incidence matrix and B_{EQ} equals the variable equality limit.

$$G^X = A_{EQ} \cdot x_{EQ} - B_{EQ} \tag{30}$$

The 1st and 2nd order partial derivatives of $G(x)$ are given in general format as:

$$\nabla G(x) = G_x = \begin{bmatrix} G_x^P & G_x^Q & G_x^V & G_x^Z & G_x^X \end{bmatrix}^T \tag{31}$$

$$\nabla^2 G(x) = \frac{\partial \left(G_x^T \cdot \lambda \right)}{\partial x}$$

$$= \frac{\partial \left(G_x^{P^T} \cdot \lambda^P \right)}{\partial x} + \frac{\partial \left(G_x^{Q^T} \cdot \lambda^Q \right)}{\partial x} + \frac{\partial \left(G_x^{V^T} \cdot \lambda^V \right)}{\partial x} + \frac{\partial \left(G_x^{Z^T} \cdot \lambda^Z \right)}{\partial x} + \frac{\partial \left(G_x^{X^T} \cdot \lambda^X \right)}{\partial x} \quad (32)$$

3) General formula of inequality constraints $H(x)$

The elements in the inequality constraint vector $H(x)$ are explained below. μ are dual variables as Lagrange multipliers

$$H(x) = \begin{bmatrix} H^f \\ H^t \\ H^{V+} \\ H^{V-} \\ H^Z \\ H^X \end{bmatrix} \leftrightarrow \begin{matrix} \mu^f \\ \mu^t \\ \mu^{V+} \\ \mu^{V-} \\ \mu^Z \\ \mu^X \end{matrix} \quad (33)$$

H^f and H^t are nonlinear constraints on branch flows at the *from* and *to* ends in terms of squared power (34) – (35) or squared current (36) – (37), depending on the system security requirements:

$$H^f = \left(S^f \right)^2 - \left(S_{\max}^f \right)^2 \quad (34)$$

$$H^t = \left(S^t \right)^2 - \left(S_{\max}^t \right)^2 \quad (35)$$

Or

$$H^f = \left(I_R^f \right)^2 + \left(I_M^f \right)^2 - \left(I_{\max}^f \right)^2 \quad (36)$$

$$H^t = \left(I_R^t \right)^2 + \left(I_M^t \right)^2 - \left(I_{\max}^t \right)^2 \quad (37)$$

$$S^f = \left(V_R^f \cdot I_R^f + V_M^f \cdot I_M^f \right) + j \left(V_M^f \cdot I_R^f - V_R^f \cdot I_M^f \right) \quad (38)$$

Where I_R^f, I_M^f, I_R^t, and I_M^t can be found using (6) – (7). V_R^f, V_M^f, V_R^t, and V_M^t are the real and imaginary parts of voltages at *from* and *to* ends of branches. The *to* end branch flow S^t can be found in a similar way.

The inequality voltage limits are evaluated only for PQ nodes ($V_{min} < V_{max}$) as nonlinear constraints in (39):

$$H^{V+} = V_R^2 + V_M^2 - V_{max}^2$$
$$H^{V+} = -(V_R^2 + V_M^2) + V_{min}^2$$
(39)

H^Z is optional customized nonlinear inequality constraint defined by user as needed. Such an example is presented in part C of this section for SST implementation.

The linear inequality constraint H^X is defined similar to its equality counterpart.

$A_{IE}^+ = -A_{IE}^-$ are incidence matrices, and B_{IE}^+ and B_{IE}^- are vectors equal to the variable upper and lower limits, respectively.

$$H^X = \begin{bmatrix} A_{IE}^+ \\ A_{IE}^- \end{bmatrix} \cdot \begin{bmatrix} x_{IE} \\ x_{IE} \end{bmatrix} - \begin{bmatrix} B_{IE}^+ \\ -B_{IE}^- \end{bmatrix}$$
(40)

The 1st and 2nd order partial derivatives of $H(x)$ are given as:

$$\nabla H(x) = H_x = \begin{bmatrix} H_x^f & H_x^t & H_x^{V+} & H_x^{V-} & H_x^Z & H_x^X \end{bmatrix}^T$$
(41)

$$\nabla^2 H(x) = \frac{\partial \left(H_x^T \cdot \mu \right)}{\partial x} = \frac{\partial \left(H_x^{f^T} \cdot \mu^f \right)}{\partial x} + \frac{\partial \left(H_x^{t^T} \cdot \mu^t \right)}{\partial x} + \frac{\partial \left(H_x^{V+^T} \cdot \mu^{V+} \right)}{\partial x}$$
$$+ \frac{\partial \left(H_x^{V-^T} \cdot \mu^{V-} \right)}{\partial x} + \frac{\partial \left(H_x^{Z^T} \cdot \mu^Z \right)}{\partial x} + \frac{\partial \left(H_x^{X^T} \cdot \mu^X \right)}{\partial x}$$
(42)

4) Build Lagrange Function

$$L(x, \lambda, \mu, s) = F(x) + \lambda^T G(x) + \mu^T (H(x) + s) - \sigma \sum \ln(s)$$
(43)

There are four variables in the Lagrange function:

x is the vector of primal independent variable.

λ and μ are vectors of Lagrange multipliers (dual variables) assigned to equality and inequality constraints.

s is a vector of slack variable.

σ is a barrier factor.

Taking partial derivatives of the Lagrange function with respect to each variable yields:

$$\nabla L(x, \lambda, \mu, s) = \begin{bmatrix} L_x & L_\lambda & L_\mu & L_s \end{bmatrix}^T \tag{44}$$

The Karush-Kuhn-Tucker (KKT) optimality conditions for the OPF problem are satisfied when the 1st order Lagrange derivatives in (44) are all equal to zero and the barrier constant γ is close to zero, also the inequality dual variable μ is nonnegative [16], which can be defined as:

$$\begin{aligned} C_1 &= \max\{G(x), H(x) + s\} \to 0 \\ C_2 &= L_x \to 0 \\ C_3 &= \mu^T \cdot s \to 0 \\ C_4 &= \min\{\mu\} \geq 0 \end{aligned} \tag{45}$$

The 2nd order derivative (Hessian) matrix of the Lagrange function is calculated in order to solve for the KKT optimality point x^*.

$$\nabla^2 L(x, \lambda, \mu, s) = \begin{bmatrix} L_{xx} & \cdots & L_{xs} \\ \vdots & \ddots & \vdots \\ L_{sx} & \cdots & L_{ss} \end{bmatrix} \tag{46}$$

Let $\chi = [x, \lambda, \mu, s]^T$, variables x, λ, μ and s are updated using the Newton-Raphson iterative method in (47) and (48). k is the iteration number.

$$\Delta\chi = \left(\nabla^2 L\right)^{-1} \cdot \left(-\nabla L\right) \tag{47}$$

$$\chi^{k+1} = \chi^k + \Delta\chi \tag{48}$$

B. Modifications from User-Defined Cost Functions

Piecewise generation costs are included as an example of customer-defined objective functions. A constrained continuous linear function f_{pw} is introduced in the previous section. The customized cost function is defined based on (9) as:

$$f_Z(x) = f_{pw}(x) = \text{price}_i (P_G - P_i) + C_{pw_i}, \ P_{i-1} \leq P_G \leq P_i \tag{49}$$

Since the partial derivatives of f_{pw} can only be evaluated in discontinuous segments, a new customized constrained variable x_{pw} is created equal to f_{pw}.

$$x_Z = x_{pw} = f_{pw}(x) \tag{50}$$

This new variable x_Z is added to the independent variable vector x as shown in (14). The dimension of x_{pw} is the total number of generations in three-phase with piecewise cost functions. The 1st and 2nd order derivatives of f_{pw} are given below:

$$\nabla f_{pw}(x) = \partial f_{pw} / \partial x = \partial f_{pw} / \partial x_{pw} = 1 \tag{51}$$

$$\nabla^2 f_{pw}(x) = 0 \tag{52}$$

The linear constraints for x_{pw}, associated with P_g will be included in H^X as in (40), and can be expressed as a linear matrix format as:

$$\begin{bmatrix} \text{price}_i & -1 \end{bmatrix} \cdot \begin{bmatrix} Pg \\ x_{pw} \end{bmatrix} \leq \begin{bmatrix} \text{price}_i \cdot P_i - C_{pwi} \end{bmatrix} \tag{53}$$

C. Modifications from SST Implementation

Because of the exclusive features introduced earlier in Section II.C, the SST implementation may change the OPF model by modifying variables and constraints. TABLE II gives a cases list of SST implementation based on the nodal elements and SST control mode. SST control mode 1 is unity power factor (UPF) that is to have zero reactive injection/consumption at the coupling point with the primary feeder; in control mode 2, SST can regulate the var injection/consumption based on external control signal sent by control center at DNO.

TABLE II
LIST OF SST IMPLEMENTATION CASES

Case	Nodal element		SST Control Mode
	Load	Generation	
1	√	X	1: unity power factor (UPF)
2	X	√	
	√	√	
3	√	X	2: var control
4	X	√	
	√	√	

The modifications of each case to OPF formulation are summarized in TABLE III. In general, SSTs will set node type to PQ node.

In case 1, the reactive injection/consumption from DER and loads are filtered out to be zero by SST. Also the nonlinearity of *ZIP* loads will be removed since the customer terminal voltage is always regulated to 1.0 per unit. These changes in case 1 are also applicable to the other cases.

In cases 2 and 4 (DER at SST node), the DER active power limit is restricted by SST capacity rating.

$$\max(-S_{SST}, P_g^{\min}) \le P_g \le \min(S_{SST}, P_g^{MAX}) \tag{54}$$

In case 3 and 4, new variables, named Q_{SST}, are added to variable x_4 as controllable reactive generation. In case 3, Q_{SST} has linear double boundary limits (55) since the active power is a constant. But in case 4, the Q_{SST} limit must address the coupling with DER active power generation in a new customized non-linear inequality constraint H^Z to satisfy SST rating (56).

$$-\sqrt{S_{SST}^2 - P_D^2} \le Q_{SST} \le \sqrt{S_{SST}^2 - P_D^2} \tag{55}$$

$$H^Z = \left(P_G - P_D\right)^2 + \left(Q_{SST}\right)^2 - \left(S_{SST}\right)^2 \tag{56}$$

TABLE III
MODIFICATION TO SYSTEM MODEL AND FORMULATION IN SST IMPLEMENTATION CASES

Case	Modifications to OPF Formulation	
1		$Q_D = 0$ $\partial S^{ZIP}/\partial V = 0$
2	• Enforce linear variable constraint for Pg by SST rating.	$Q_D = 0$ $\partial S^{ZIP}/\partial V = 0$
3	• Add new variable Q_{SST} to x_4 with new linear variable constraint	$Q_D = 0$ $\partial S^{ZIP}/\partial V = 0$
4	• Enforce linear variable constraint for Pg by SST rating. • Add new variable Q_{SST} to x_4 with new nonlinear inequality constraint	$Q_D = 0$ $\partial S^{ZIP}/\partial V = 0$

D. Novel Control Scheme

Fig. 3 illustrates a novel infrastructure and control scheme for the envisioned smart grid distribution system. DERs are integrated through the plug-and-play hub (LVDC) in the SST. The DNO can collect measurement and status of DERs, loads, and SSTs through a digitalized communication platform. These data enables the DNO to perform optimization, such as three-phase OPF, and send out signals to the controllable resources and devices. The OPF can be used to determine the active power generation dispatch of transmission supply ($P_{g,1}^*$) and DERs ($P_{g,2}^*$ and $P_{g,3}^*$), as well as the reactive power injections (Q_{SST}^*) to SSTs that are operating in var control mode. Though not addressed explicitly in this paper, demand response control (S_d^*) can also be determined using the proposed OPF. It is possible to integrate multiple control algorithms, such as state estimation, energy storage operation, and voltage regulation, etc. This control scheme can also be extended to real-time control.
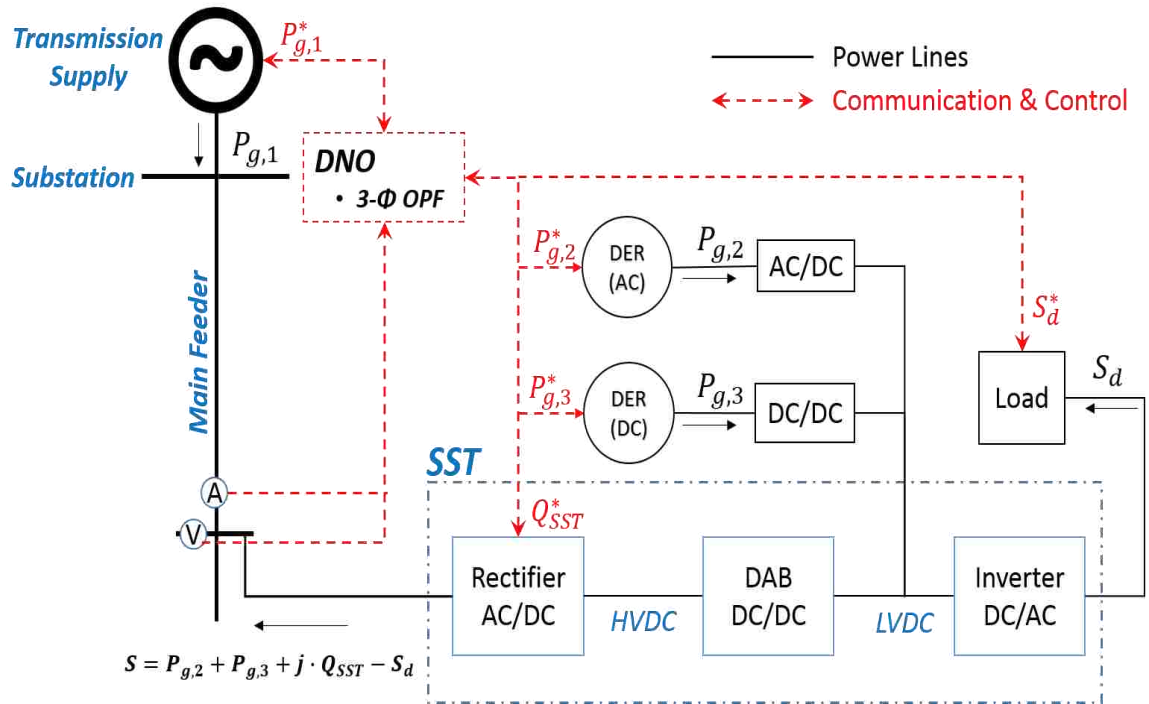
Fig. 3 Novel distribution system control with DER and SST implementation.

IV. TEST RESULTS

A. Modified IEEE-34 Test Feeder

The IEEE-34 test feeder is a benchmark unbalanced test system consisting of high r/x ratio conductors and nonlinear *ZIP* loads. This system is modeled in the OPF algorithm based on [22], except for the integration of DERs and SSTs at specified nodes. Three DER units are installed at nodes 822, 848 and 890, purposely located close to nodes with large loads and low voltages (e.g. 0.9167 pu at node 890-A [22]). Two capacity size settings of DERs (approximately 40% and 90% of total rated load) are given in TABLE IV for different test cases. DER costs use piecewise functions that are designed with reasonable values to create various price levels that are comparable to the quadratic cost function from the aggregated transmission side generation. DER costs on different phases at the same node are assumed the same in this test.

The aggregated supply from transmission network acts as a slack node at substation − node 800. The generation cost is a quadratic function and the polynomial factors are shown in TABLE V. There are a total of five SSTs installed on system (see TABLE VI). Two of them are located at nodes 844 and 860, and the other three are at DER nodes 822, 848, and 890. The capacity ratings of each SST is determined based on the size of the local load and total DER available at the node. Test cases are defined in TABLE VII based on DER capacity rating and SST control mode. The nodal voltage magnitude constraint is set between 0.925 to 1.075 pu. Voltage regulators at nodes 814 and 852 have zero tap position setting in this test. The results are compared and discussed next.

The diagram of the modified IEEE-34 is shown in Fig. 4.

TABLE IV
GENERATION COST OF DERs IN MODIFIED IEEE-34
(ACTIVE POWER P IN kW, PRICE IN \$/MWH)

Low DER Rating							
Node	*Pmax*	P_1	Price$_1$	P_2	Price$_2$	P_3	Price$_3$
822	40	25	18	24	20	40	28
848	160	70	15	144	21	160	27
890	160	50	19	120	22	160	26
High DER Rating							
Node	*Pmax*	P_1	Price$_1$	P_2	Price$_2$	P_3	Price$_3$
822	75	30	18	45	20	75	28
848	300	150	15	270	21	300	27
890	300	110	19	225	22	300	26

TABLE V
GENERATION COST OF TRANSMISSION SUPPLY IN MODIFIED IEEE-34
(ACTIVE POWER P IN kW)

Node	*Pmax*	a_0	a_1	a_2
800	3000	150	25	0.25

TABLE VI
SST LOCATION AND RATING IN MODIFIED IEEE-34

Node	S_{SST}-A (kVA)	S_{SST}-B (kVA)	S_{SST}-C (kVA)
844	220	220	220
860	140	140	140
822	80	N/A	N/A
848	440	440	440
890	440	440	440

TABLE VII
LIST OF TEST CASES IN MODIFIED IEEE-34

	No SST	SST mode 1	SST mode 2
Low DER Rating	Test 1.*a*	Test 1.*b*	Test 1.*c*
High DER Rating	Test 2.*a*	Test 2.*b*	Test 2.*c*
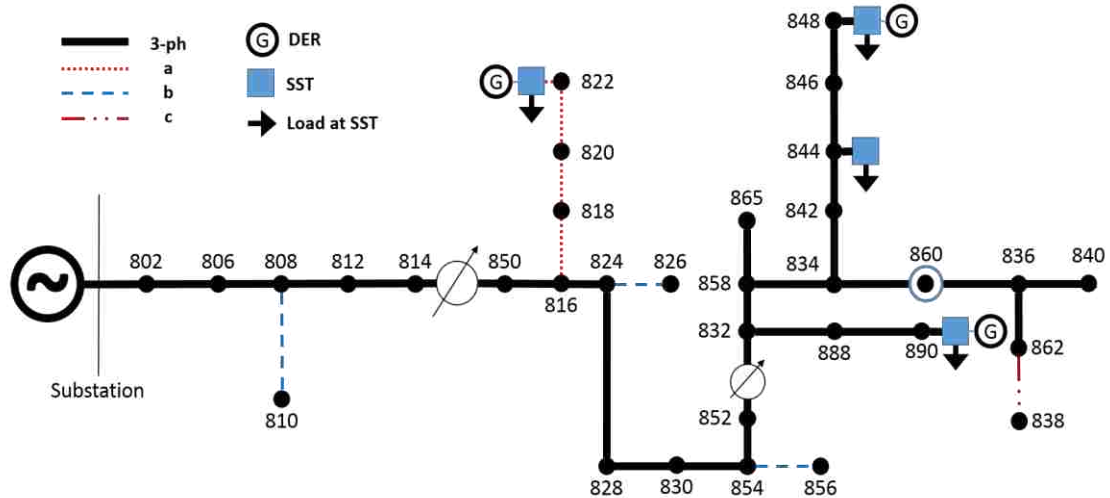
Fig. 4 Modified IEEE-34 test feeder with integrated DERs and SSTs.

B. Results of Tests 1 and 2

- Test 1

The OPF algorithm can solve generation outputs for minimum system total generation cost under different system configurations and operating models. The power injections as well as the nodal active power shadow prices are given at the generation and/or the SST nodes in TABLE VIII. TABLE IX compares some of these results.

Test 1.*a* is the basic case with low DER penetration and no SST installation. Generation dispatch is solved by OPF while satisfying system constraints, such as voltage magnitude limits. The DER at node 890-A is injecting at less economic price segment ($26/h) in order to maintain the nodal phase voltage above the lower constraint of 1.025 pu, without any help from voltage regulators.

After installing SSTs in the UPF mode (Test 1.*b*), the system total rated reactive demand decreased more than 60% on each phase. The minimum nodal voltage is raised

from 0.925 pu at 890-A to 0.997 pu at 822-A. Despite the desirable voltage boost, the equivalent active loads are increased due to the non-linearity of *ZIP* loads. Therefore the DER at 890 is dispatched at full capacity of 160 kW since the nodal shadow prices at 890 are higher than the highest price of DER 890, which is 26$/h.

In test 1.*c*, the SSTs at nodes 848 and 844 are commanded to absorb large quantities of reactive power. So the system voltages are regulated towards unity resulting in a slight reduction of several kW of the equivalent *ZIP* load. The transmission power supply and the slack node shadow prices – which are commonly used as system reference price in economic operation –are reduced as compared to test 1.*b*. It is also noticed that the overall system active power loss in test 1.*c* is lower than the other two cases, which may be attributed to the benefits of optimized control of DER and SST.

TABLE VIII
RESULTS OF P_G (KW), Q_{SST} (KVAR) AND SHADOW PRICE $\varLambda^P$ ($/H) IN TEST 1

Node	Phase	1.a		1.b		1.c		
		P_g	λ^P	P_g	λ^P	P_g	λ^P	Q_{SST}
800	A	342.30	25.17	344.57	25.17	314.67	25.16	N/A
	B	330.68	25.17	313.46	25.16	283.50	25.14	
	C	279.93	25.14	262.03	25.13	242.96	25.12	
822	A	24.00	26.78	24.00	27.31	24.00	27.41	15.16
848	A	144.00	25.61	144.79	26.97	159.50	27.13	-145.44
	B	144.00	25.18	144.68	26.98	158.65	27.06	-139.44
	C	144.00	23.72	144.00	26.30	144.12	26.91	-147.91
890	A	133.67	26.00	160.00	26.72	159.97	26.82	-0.38
	B	120.00	24.35	160.00	26.68	159.97	26.70	-0.73
	C	119.89	22.28	159.43	26.08	159.98	26.54	-0.61
844	A	N/A	25.65	N/A	27.02	N/A	27.18	-89.75
	B		25.21		27.01		27.10	-106.11
	C		23.76		26.34		26.95	-112.61
860	A		25.68		27.04		27.20	14.47
	B		25.24		27.02		27.11	19.05
	C		23.78		26.36		26.96	1.37

TABLE IX
RESULTS COMPARISON IN TEST 1 CASES

Test	Phase	Vmax (pu)	at node	Vmin (pu)	at node	Total Pd (kW)	Total Qd (kVar)	Ploss%
1.a	A	1.050	800	0.925	890	618.19	397.82	3.498
	B	1.050	800	0.935	890	571.38	335.96	
	C	1.050	800	0.948	890	530.55	279.48	
1.b	A	1.050	800	0.997	822	647.18	127.85	4.087
	B	1.050	800	1.031	838	589.86	110.77	
	C	1.050	800	1.035	862	544.02	61.86	
1.c	A	1.050	800	0.983	862	643.85	125.37	2.134
	B	1.050	800	1.001	838	586.92	109.26	
	C	1.050	800	0.990	840	537.98	60.36	

- Test 2

Conventional distribution systems do not allow very high DER integration mainly due to security concerns and the lack of control. In Test 2, however, the OPF program is able to aggregate energy production from DERs in an optimized fashion while satisfying the security conditions. In Test 2.a (see TABLE X), the high levels of DER penetration make DER-890 the marginal generation, which means the nodal shadow prices at node 890 is determined by this DER. The minimum voltages are also higher compared to the small DER case in Test 1.a.

When the installed SSTs are operated at UPF mode, the output at marginal DER890 increases to serve the equivalent *ZIP* load similar to the case of Test 1.*b*. However, in Test 2.*b*, since the voltage level at node 890 is already at the upper limit (see TABLE XI) due to reversed power flow from DER injections, the DER890 cannot continue to inject more active power while there is still some reserve capacity at the same price segment.

The above problem can be mitigated by optimally controlling the var support at the SSTs through the OPF program. The voltage constraints are relieved as a result of the var absorption at SSTs 848 and 844, so that the DER890 is now fully dispatched at 225 *kW* within the cheaper price segment. The transmission power injections and shadow prices at the substation are the lowest in the cases studied in Test 2. The total system P_{loss} is also reduced to 0.771% because of low level of branch flow along the feeder.

It is observed from both Tests 1 and 2 that the active power generation or demand may significantly affect the system nodal voltages especially in a network consisting of high r/x ratio conductors. This fact makes it more important to have adequate controllable

distributed reactive power resources – such as SSTs – in order to counter balance the impact from DER active power penetration while maintaining voltage security.

Although not included in this paper, further modification can be done to incorporate voltage regulator tap positions as new user-defined independent variables in the OPF that could further improve system efficiency and economy by coordinating with DER and SSTs.

TABLE X
RESULTS OF P_G (KW), Q_{SST} (KVAR) AND SHADOW PRICE Λ^P ($/H) IN TEST 2

Node	phase	2.a		2.b		2.c		
		P_g	λ^P	P_g	λ^P	P_g	λ^P	Q_{SST}
800	A	205.30	25.10	165.40	25.08	113.69	25.06	N/A
	B	195.53	25.10	162.14	25.08	104.89	25.05	
	C	167.78	25.08	131.56	25.07	50.49	25.03	
822	A	45.00	25.10	45.00	25.45	45.00	25.80	11.59
848	A	270.00	22.95	270.00	23.96	270.00	24.61	-157.62
	B	270.00	23.30	270.00	24.16	270.00	24.77	-152.34
	C	270.00	22.57	270.00	23.79	270.00	24.37	-160.90
890	A	129.93	22.00	186.54	22.00	225.00	23.14	2.05
	B	136.57	22.00	181.82	22.00	225.00	23.23	0.68
	C	114.30	22.00	162.39	22.00	225.00	22.88	1.00
844	A	N/A	23.03	N/A	24.03	N/A	24.69	-102.01
	B		23.36		24.22		24.83	-117.56
	C		22.64		23.85		24.44	-130.72
860	A		23.06		24.06		24.72	13.53
	B		23.39		24.24		24.85	19.33
	C		22.67		23.88		24.47	-1.46

TABLE XI
RESULTS COMPARISON IN TEST 2 CASES

Test	Phase	Vmax (pu)	at node	Vmin (pu)	at node	Total Pd (kW)	Total Qd (kVar)	Ploss%
2.a	A	1.050	800	0.956	890	638.73	412.99	1.599
	B	1.050	800	0.973	890	589.38	347.39	
	C	1.050	800	0.967	890	547.31	288.17	
2.b	A	1.075	890	1.025	822	654.10	132.97	2.652
	B	1.075	890	1.050	800	593.04	112.41	
	C	1.075	890	1.050	800	548.77	63.02	
2.c	A	1.068	890	1.012	822	650.42	130.23	0.771
	B	1.074	890	1.040	838	590.63	111.17	
	C	1.074	890	1.036	862	544.14	61.89	

C. Modified IEEE-123 Test Feeder

The IEEE-123 test feeder is another standard unbalanced test system. The original system has been modified by installing DERs at nodes 66, 51, 76, and 30, and SSTs at nodes 66, 51, 76, 30, 13, and 60. Fig. 5 shows the diagram of the modified IEEE-123 system. The capacity and energy cost of DERs and transmission supply are listed in TABLE XII and TABLE XIII. It should be noticed that the original loads are highly unbalanced, as loads on phase A and C are approximately 55% and 23% higher than the load on phase B, respectively. So each DER has a different capacity in cost segments on each phase. Consequently, the SSTs are also installed with different capacity ratings on each phase, as shown in TABLE XIV. Study cases are listed in TABLE XV.

The nodal voltage magnitude constraint is set between 0.95 to 1.05 pu. The voltage regulator at substation 150 has reduced taps of 5 on each phase, and the other regulators at 9-14, 25-28, 60-67 have zero tap setting in this test. The results are compared and discussed next.
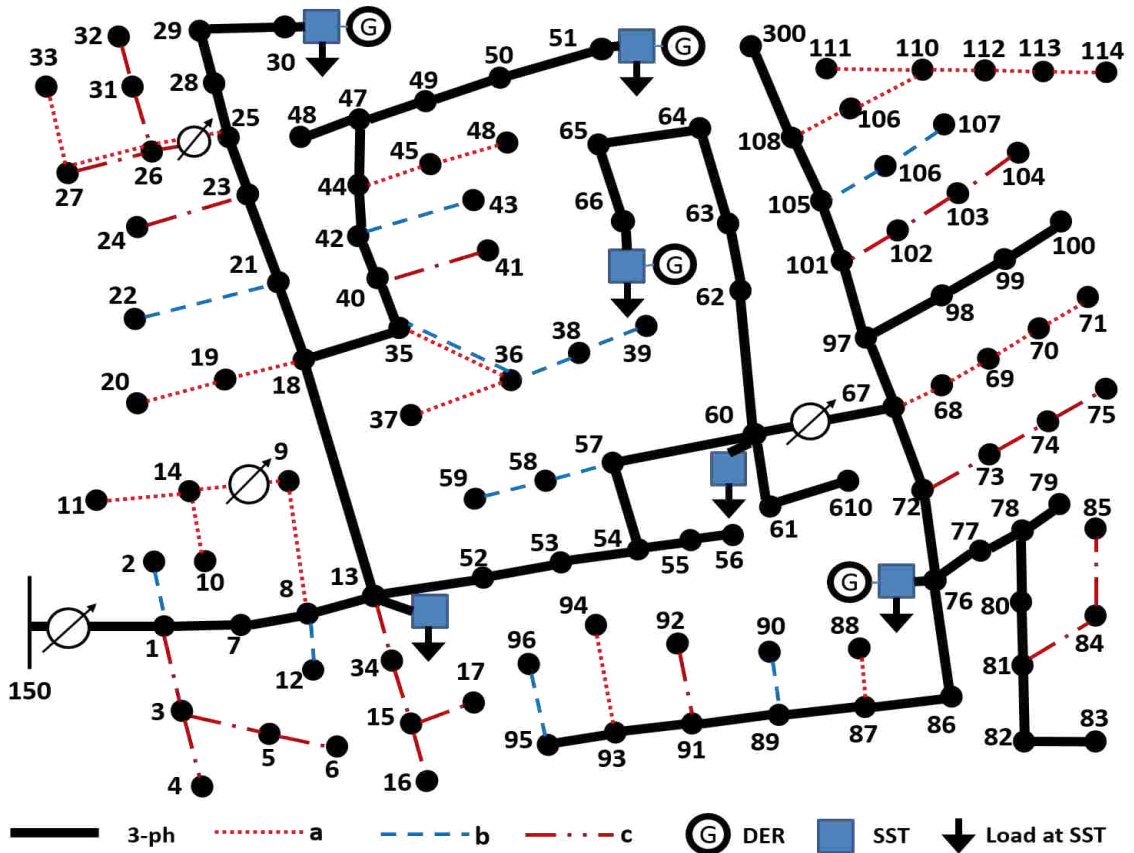
Fig. 5 Modified IEEE-123 test feeder with integrated DERs and SSTs.

TABLE XII
GENERATION COST OF DERs IN MODIFIED IEEE-123
(ACTIVE POWER *P* IN kW, PRICE IN $/MWh)

Node	Phase	*Pmax*	P_1	Price$_1$	P_2	Price$_2$	P_3	Price$_3$
	A	522	296	15	470	20	522	32
66	B	360	204	15	324	20	360	32
	C	432	245	15	389	20	432	32
	A	487	261	13	435	21	487	23
51	B	336	180	13	300	21	336	23
	C	403	216	13	360	21	403	23
	A	470	244	16	383	24	470	27
76	B	324	168	16	264	24	324	27
	C	389	202	16	317	24	389	27
	A	360	90	20	252	23	360	28
30	B	240	60	20	168	23	240	28
	C	288	72	20	202	23	288	28

TABLE XIII
GENERATION COST OF TRANSMISSION SUPPLY IN THE MODIFIED IEEE-123
(ACTIVE POWER P IN KW)

Node	$Pmax$	$Pmin$	a_0	a_1	a_2
150	2000	-2000	140	25.5	0.24

TABLE XIV
SST LOCATION AND RATING IN THE MODIFIED IEEE-123

Node	S_{SST}-A (kVA)	S_{SST}-B (kVA)	S_{SST}-C (kVA)
66	600	400	480
51	540	360	430
76	520	350	420
30	400	260	300
13	300	200	240
60	300	200	240

TABLE XV
LIST OF TEST CASES IN MODIFIED IEEE-123

No SST	SST mode 1	SST mode 2
Test 3.a	Test 3.b	Test 3.c

D. Results of Test 3

Test 3 shows extreme cases of high DER penetration and reversed gateway active power flow at the substation node. From the economic dispatch results (see TABLE XVI), the total generation from DERs is higher than the total demand which results in negative active power flow at the substation node. The substation absorbs active power and appears like a co-gen to the bulk power network. The DNO aggregates cheaper energy from DERs and sells power in the wholesale market.

DER-76 is the marginal generation dispatched at a price of $24/hour. The shadow prices (λ^P) appear generally lower near the DER node and higher near the substation due to reversal of the power flow.

Since the optimal solutions of OPF are within security constraints and the implementation of SSTs does not affect the constraint conditions (see TABLE XVII), the generation dispatch of DERs in all three cases are identical. However, in case 3.c, SSTs at var control mode does help increase the total active power available at the substation for selling back to the bulk energy market without changing DER active power injections. Combined with cases 1 and 2, a general conclusion can be made that the SSTs as controllable var sources can improve system operation with maximum economic benefits and improve voltage regulation at the same time.

TABLE XVI

RESULTS OF P_G (KW), Q_{SST} (KVAR) AND SHADOW PRICE Λ^P ($\$/H$) IN TEST 3

Node	Phase	3.a		3.b		3.c		
		P_g	λ^P	P_g	λ^P	P_g	λ^P	Q_{SST}
150	A	-147.8	25.43	-147.3	25.43	-155.6	25.42	N/A
	B	-135.2	25.43	-134.8	25.43	-136.8	25.43	
	C	-128.5	25.44	-127.5	25.44	-134.3	25.43	
66	A	469.8	23.42	469.8	23.43	469.8	23.65	32.5
	B	324.0	24.52	324.0	24.66	324.0	24.44	50.3
	C	388.8	24.16	388.8	24.20	388.8	24.11	-29.5
51	A	487.2	24.43	487.2	24.44	487.2	24.46	-52.8
	B	336.0	24.70	336.0	24.74	336.0	24.74	-62.3
	C	403.2	24.71	403.2	24.74	403.2	24.66	-56.7
76	A	382.8	24.51	382.8	24.61	382.8	24.87	-207.4
	B	264.0	25.35	264.0	25.55	264.0	25.37	-134.3
	C	316.8	24.82	316.8	24.86	316.8	24.86	-332.2
30	A	252.0	24.63	252.0	24.63	252.0	24.66	-110.3
	B	168.0	24.74	168.0	24.80	168.0	24.84	-15.7
	C	201.6	25.01	201.6	25.03	201.6	24.93	22.1
13	A		25.01		25.02		25.09	-91.7
	B		25.12		25.16		25.13	-16.8
	C	N/A	25.12	N/A	25.14	N/A	25.10	-36.4
60	A		24.59		24.63		24.82	15.8
	B		25.15		25.25		25.09	-102.4
	C		24.84		24.87		24.85	-36.5

TABLE XVII
RESULTS COMPARISON IN TEST 3 CASES.

Test	Phase	Vmax	at node	Vmin	at node	Total Pd kW	Total Qd kVar	Ploss%
3.a	A	1.0379	66	0.9954	114	1420.33	759.72	1.063
	B	1.0313	150	1.0117	96	951.07	569.77	
	C	1.0403	66	1.0240	104	1168.84	620.91	
3.b	A	1.0424	66	1.0019	114	1422.19	686.00	1.011
	B	1.0351	83	1.0200	47	951.31	494.32	
	C	1.0484	66	1.0268	6	1170.71	516.46	
3.c	A	1.0313	150	0.9740	114	1404.97	675.78	1.602
	B	1.0317	66	1.0084	107	948.21	492.50	
	C	1.0313	150	0.9800	104	1150.26	505.85	

V. CONCLUSIONS

The increasing installation of distributed energy resources along with new investments on infrastructure improvement packs the promise to enable the aging distribution system to evolve into a smart grid paradigm with increased controllability. A generalized three-phase unbalanced OPF algorithm is proposed to perform optimization control by an entity, such as the DNO to aggregate the profitability of each resource while satisfying security constraints. The algorithm structure is general enough to adopt new user-defined device models and constraints. As one example of customization, an SST with its purported functionalities is included in the OPF algorithm to demonstrate the optimal control scheme in distribution systems with high levels of DER penetration. The feature of reactive var injection control at the SST is an important instrument to support DER penetration and renewable energy harvesting, especially in distribution

networks featuring high r/x ratio conductors. Based on results obtained by the OPF applied to an IEEE test feeders, the coordination between DER and SST in var control mode presents the most potential benefits of economic operation, voltage regulation, and system efficiency improvements.

The proposed OPF algorithm also presents potential value in system optimal design and restructuring. Extended research can be conducted on:

- Including voltage regulator as control variable

- Demand response and energy storage coordination

- Including voltage regulation as an optimization objective.

REFERENCES

[1] "Grid 2030: A National Vision for Electricity's Second 100 Years Jul 2007," Office of Electric Transmission and Distribution, U.S. Dept. of Energy [Online]. Available: http://en ergy.gov/

[2] N. Hadjsa ïd and J. Sabonnadi ère, *Power Systems and Restructuring*. London, Wiley, 2009.

[3] U.S. Department of Energy, "2010 Smart Grid System Report," Feb 2012 [online]. Available: https://www.smartgrid.gov/

[4] Energy Regulatory Commission (CRE) in France. Available online: http://www.cre.fr/en

[5] International Renewable Energy Agency, "Renewable Energy Technologies: Cost Analysis Series," vol. 1, no. 4/5, June 2012.

[6] "The potential benefits of distributed generation and rate-related issues that may impede their expansion," U.S. D.O.E, Feb. 2007 [online]. Available: http://www.energy.gov

[7] A.Q. Huang, M.L. Crow, G.T. Heydt, J.P. Zheng, and S.T. Dale, "The future renewable electric energy delivery and management," *Proc. IEEE*, vol. 99, no. 1, pp. 133–148, Jan. 2011.

[8] E. R. Ronan, S. D. Sudhoff, S. F. Glover, and D. L. Galloway, "A power electronic-based distribution transformer," *IEEE Transactions on Power Delivery*, vol, 17, no. 2, pp 537--547, April 2002.

[9] X. She, A. Q. Huang, and R. Burgos, "Review of the solid state transformer technologies and its application in power distribution system," *IEEE Journal of Emerging and Selected Topics in Power Electronics*, early access, 2013.

[10] H. Qin and J. W. Kimball, "Solid-state transformer architecture using ac-ac dual-active-bridge converter," *IEEE Transactions on Industrial Electronics*, vol. 60, no. 9, pp. 3720-3730, 2013.

[11] X. She, A. Q. Huang, S. Kukic, and M. E. Baran, "On integration of solid-state transformer with zonal dc microgrid," *IEEE Transactions on Smart Grid*, vol. 3, no. 2, pp. 975--985, 2012.

[12] D. Shah and M. Crow, "Stability Design Criteria for Distribution System with Solid State Transformers," *IEEE Transactions on Power Delivery*, early access, Apr 2014.

[13] J. Sun, M. Chen, and K. J. Karimi, "Analysis and mitigation of system interactions involving single-phase PFC converters," *IEEE Transactions on Aerospace and Electronic Systems*, vol. 44, no. 1, pp. 217--226, 2008.

[14] Power Systems Engineering Research Center, "The 21st Century Substation Design – Final Project Report," *PSERC Publication 10-15*, Sep 2010 [online]. Available: http://www.pserc.wisc.edu/

[15] T. Zhao, L. Yang, J. Wang, and A. Huang, "270 kVA Solid State Transformer Based on 10 kV SiC Power Devices," *IEEE Electric Ship Technologies Symposium,* May 2007.

[16] A. Forsgren, P. E. Gill, M. H. Wright, "Interior Methods for Nonlinear Optimization," *Society for Industrial and Applied Mathematics Review*, vol. 44, no. 4, pp. 525-597, Oct, 2002.

[17] P. Garcia, J. Pereira, S. Carneiro, Jr., V. Costa and N. Martins, "Three-Phase Power Flow Calculations Using the Current Injection Method," *IEEE Transactions on Power System*, vol. 15, no. 2, May 2000.

[18] R. Byrd, J. Nocedal, R. Waltz, and Y. Wu, "On the Use of Piecewise Linear Models in Nonlinear Programming," *Mathematical Programming,* vol. 137, no. 1-2, pp. 289 − 324, Feb 2013.

[19] F. Meng, D. Haughton, B. Chowdhury, M. Crow, and G. Heydt, "Distributed Generation and Storage Optimal Control with State Estimation," *IEEE Transactions on Smart Grid,* vol. 4, no. 4, Dec 2013.

[20] W. H. Kersting, *Distribution System Modeling and Analysis*. New York: CRC, 2007.

[21] F. Wang, X. She, G. Wang, A. Huang, and R. Burgos, "Parallel Operation of Solid State Transformer," *ECCE, IEEE,* 2012.

[22] IEEE PES Distribution System Analysis Subcommittee's Distribution Test Feeder Working Group [online].
Available: http://www.ewh.ieee.org/soc/pes/dsacom/testfeeders/index.html

SECTION

2. CONCLUSION

In this dissertation, a three-phase PDIPM based OPF program is proposed as a fundamental analyzing tool for DNO optimization control in a future smart distribution system with high levels of DERs. This novel control scheme is carried out in three parts:

In the first paper, a balanced OPF coordinating with an energy storage management algorithm is proposed using a distribution locational marginal pricing (DLMP) index. This control scheme provides potential improvement for renewable energy harvest and economic benefits to both the customers and the utility in the day-ahead operation planning of DER and DES.

In the second paper, an unbalanced three-phase OPF algorithm is developed and tested for providing economic dispatch of transmission and DER suppliers in an assumed competitive environment. The algorithm shows fast convergence under various system configurations and is capable to solve for line loading management and generation re-dispatch in a looped or meshed system topology.

An enhanced OPF formulation is presented in the third paper with adaptability to incorporate new customized devices or constraints by modifying the variables, constraints and even objective functions. Such example is presented by integrating SST as controllable var sources into OPF algorithm. The coordination of DER and SST in var control mode provide maximum potential benefits in economic operation and voltage regulation.

The proposed OPF program can be implemented for use by the DNO with other control methods, such as energy storage management using dynamic programming, to

aggregate maximum energy profitability from each of the available sources. This novel control scheme also shows potential application in short or long term system optimal design by simply substituting the objective function with planning cost minimization.

VITA

Fanjun Meng was born in Luoyang, China. He received his B.E. in Electrical Engineering from Shanghai Jiaotong University, China, in July 2007. He started his study and research towards Ph.D. degree at Missouri University of Science and Technology, Rolla, Missouri, USA, from August 2008 and received his Ph.D. in Electrical Engineering in August 2014. He worked as a graduate researcher and served as a member of student leader council in the Future Renewable Electric Energy Delivery (FREEDM) Systems Center from 2008 to 2013.

He has published conference and journal papers, some of which are listed with the references of this research

He has been a student member of IEEE and IEEE Power Engineering Society since 2009. He is also a member of IEEE Eta Kappa Nu (HKN) since 2008. His major research interests include optimal power flow analysis for balanced and unbalanced power systems, distributed energy resources integration, energy storage management, energy market and regulatory.